

BRIGHT X-RAY SOURCES IN M31 GLOBULAR CLUSTERS

R. DI STEFANO, A.K.H. KONG, M. R. GARCIA, P. BARMBY

Harvard-Smithsonian Center for Astrophysics, 60 Garden Street, Cambridge, MA 02138

J. GREINER

Astrophysical Institute Potsdam, 14482 Potsdam, Germany

S.S. MURRAY, F.A. PRIMINI

Harvard-Smithsonian Center for Astrophysics, 60 Garden Street, Cambridge, MA 02138

Draft version February 7, 2020

ABSTRACT

We have conducted *Chandra* observations of ~ 900 square arcmin (~ 46 kpc 2) of M31, and find that the most luminous X-ray sources in most of our fields are in globular clusters. Of the 30 globular cluster X-ray sources in our fields, 17 are newly discovered. Approximately 1/3 of all the sources have $L_x([0.5-7]\text{keV}) > 10^{37}$ ergs s $^{-1}$; approximately 1/10 of all the sources have $L_x([0.5-7]\text{keV})$ close to or above 10^{38} ergs s $^{-1}$. The most luminous source, in the globular cluster Bo 375, is consistently observed to have L_x greater than 2×10^{38} ergs s $^{-1}$.

- (1) We present data on the spectra and/or light curves of the 5 most luminous M31 globular cluster sources.
- (2) We explore possible explanations for the high X-ray luminosities of the brightest sources. These include that the X-ray sources may be composites, the radiation we receive may be beamed, metallicity effects could be at work, or the sources may be accreting black holes. We weigh each of these possibilities against the data. In addition, we introduce a neutron star model in which mass transfer proceeds on the thermal time scale of the donor star. Our model can produce luminosities of several times 10^{38} ergs s $^{-1}$, and leads to a set of well-defined predictions.
- (3) We compute the X-ray luminosity function and the distribution of counts in wavebands that span the range of energies to which *Chandra* is sensitive. We find the peak X-ray luminosity is higher and that systems with $L_x > 10^{37}$ erg s $^{-1}$ constitute a larger fraction of all GC sources than in our Galaxy.
- (4) We study the possible reasons for this difference between M31 and Galactic globular cluster X-ray sources and identify three promising explanations.

Subject headings: galaxies: individual (M31) — globular clusters: general — X-rays: galaxies — X-rays: stars

1. INTRODUCTION

1.1. X-Ray Sources in Galactic and M31 Globular Clusters

1.1.1. Galactic Globular Cluster X-Ray Sources

X-ray studies of Milky Way (MW) globular clusters (GCs) suggested that they be divided into “bright” ($L_x > 10^{35}$ ergs s $^{-1}$) and “dim” ($L_x < 10^{34}$ ergs s $^{-1}$) sources (see e.g. Hertz & Grindlay 1983; Verbunt et al. 1985; Deutsch et al. 2000). The majority of dim sources are thought to be accreting white dwarfs (Di Stefano & Rappaport 1994; Hakala et al. 1997; Grindlay et al. 2001). *Chandra* observations with realistic exposure times can only see evidence of large populations of dim sources in M31, not individual sources. We can therefore draw comparisons only between the bright GC sources in each galaxy. Twelve MW GCs house bright X-ray sources; no cluster is known to have more than a single bright source. There is evidence, largely from X-ray bursts, that the bright MW GC sources are accreting neutron stars. There is no evidence that any MW GC harbors an accreting black hole. Indeed, this apparent lack of black holes in MW GC has been commented upon and explained as perhaps due to large kick velocities obtained by BH binaries upon interactions with other GC members (Sigurdsson & Hernquist 1993; Kulkarni et al. 1993). The most luminous MW GC X-ray source (4U 1820-30 in NGC 6624) has $L_x \sim 1-5 \times 10^{37}$ ergs s $^{-1}$ (see Bloser et al. 2000 for a review).

1.1.2. M31 Globular Cluster X-Ray Sources

We have conducted *Chandra* observations of ~ 900 square arcmin (~ 46 kpc 2) of M31, and find that the most luminous X-ray sources in most of our fields are in globular clusters. Of the 30 globular cluster X-ray sources in our fields, 17 are newly discovered. Approximately 1/3 of all the sources have $L_x([0.5-7]\text{keV}) > 10^{37}$ ergs s $^{-1}$; approximately 1/10 of all the sources have $L_x([0.5-7]\text{keV})$ close to or above 10^{38} ergs s $^{-1}$. The most luminous source, in the globular cluster Bo 375, is consistently observed to have L_x greater than 2×10^{38} ergs s $^{-1}$. Given the sensitivity of the detectors we used (ACIS-S and ACIS-I), and our exposure times (15 ksec and 8.8 ksec, respectively), we could have detected sources with luminosities as low as $1.5-5 \times 10^{35}$ ergs s $^{-1}$, and indeed have discovered some sources only slightly brighter than these limits. The large fraction of globular cluster sources with $L_x > 10^{37}$ ergs s $^{-1}$ stands in sharp contrast with the situation in the Galaxy, where, e.g., only one of the 11 bright sources studied in the *ROSAT* all-sky survey had $L_x > 10^{37}$ ergs s $^{-1}$ (Verbunt et al. 1995).

Each of the following subsections (§1.2–1.6) provides an overview of the corresponding section (§2–6) of the paper.

1.2. Bo 375: the highest-luminosity X-ray source in a globular cluster

While conducting a census of M31 X-ray sources, we found that the most luminous source in our census was associated with the globular cluster Bo 375. Our observations were performed

using the ACIS-S detector aboard the *Chandra* X-Ray Observatory. The uncertainty in the position of the source is $\sim 1''$, comparable to the uncertainty in the cluster position from the Bologna catalog (Battistini et al. 1997). Since the density of X-ray sources in the region around the source is not very high (there is just one other source with $L \sim 10^{36}$ erg s $^{-1}$ within 5'), it is likely that the X-ray source is physically associated with Bo 375. The measured luminosity (between 0.5 and 2.4 keV) of this source is between $\sim 2 - 5 \times 10^{38}$ ergs s $^{-1}$. In §2 we present new data on the flux, spectrum, and light curve of the X-ray source, Bo 375. In addition, we place these observations in perspective by summarizing and, in some cases re-analyzing, data from previous X-ray observations of the source. Although the spectrum and/or light curve of Bo 375 was studied in 2 earlier papers (Supper et al. 1997; Irwin & Bregman 1999), the source luminosity is not quoted in the literature. We find, however, that, like our own observation, all previous observations of the X-ray flux, which is variable, are consistent with luminosities that range from $\sim 2 \times 10^{38}$ ergs s $^{-1}$ to $\sim 5 \times 10^{38}$ ergs s $^{-1}$. That is, barring beaming effects, the luminosity is most likely super-Eddington for a $1.4 M_{\odot}$ accretor. This would make Bo 375 X-1 an interesting source whatever its location, but its position within or very near to a globular cluster (GC) makes it even more special. This is because, as mentioned above, the maximum luminosity observed for a MW GC X-ray source is 4 times smaller than the minimum luminosity found for Bo 375. In §2 we also explore possible physical reasons for the observed high luminosity of this source.

1.3. Other Bright M31 GC X-Ray Sources

The second and third most luminous X-ray sources in our sample are also associated with globular clusters, and one of these sources also exhibits X-ray luminosity close to 10^{38} ergs s $^{-1}$. The fields we were surveying are shown in Figure 1, superposed on an optical image of M31. Because the existence of several luminous sources suggests a more general phenomenon, we have considered an additional data set, collected during 1999 and 2000 by the combination of *Chandra*'s HRC, ACIS-I, and ACIS-S. The combined data sets include 10 globular cluster X-ray sources with $L_x > 10^{37}$ ergs s $^{-1}$. The spectra and light curves of 4 of these sources are presented in §3. The light curves of these sources (and also of Bo 375), exhibit enough structure on short time scales that it is clear that at least one source in the cluster must have a luminosity that is a significant fraction of the total luminosity we have observed.

1.4. Population Studies

These high-luminosity sources raise questions about possible differences between the luminosity function of globular cluster X-ray sources in M31 and that of the Milky Way. We therefore, in §4, construct the luminosity function of the M31 globular cluster X-ray sources as measured by *Chandra*, and compare it to the luminosity function of Milky Way globular cluster sources detected during the *ROSAT* all-sky survey (Verbunt et al. 1995).

1.5. M31's Globular Clusters

The primary differences between the population of X-ray sources in M31 globular clusters and those in Galactic globular clusters are that (1) the peak luminosity is higher, and (2) the

high-luminosity end of the distribution function is more populated. It is natural to ask if these differences can be explained by differences in the two galaxies' populations of globular clusters. This question is addressed in §5.

1.6. Conclusions: Possible Explanations

Explanations are required at two levels: (1) what is the nature of the sources that appear to be so highly luminous? (2) what properties of M31 and its system of globular clusters generate these bright sources? These issues are the focus of §6.

2. BO 375

2.1. Observations and Data Reduction

Bo 375 has been observed by several X-ray missions. A summary of the X-ray observations used here is given in Table 1. Bo 375 was first observed with *Einstein* in 1979 during a survey of M31 and then it frequently appeared in the *ROSAT* M31 survey data from 1991 to 1994. It was also observed with *ASCA* in 1993 and *Chandra* in 2000 and 2001. We therefore have observations spanning an interval of more than 20 years, and can study the spectrum and the time evolution of the source.

2.1.1. Einstein Data

Bo 375 was observed with *Einstein* High Resolution Imager (HRI) in 1979 during M31 survey observations. The *Einstein* HRI has a spatial resolution of $\sim 3''$, and no spectral resolution. The count rate was extracted from a $18''$ radius circle centered on the source centroid and the count rate is ~ 0.03 counts s $^{-1}$, corresponding to $\sim 5 \times 10^{38}$ ergs s $^{-1}$ in 0.5–10 keV (assuming a power-law model with $N_H = 10^{21}$ cm $^{-2}$, $\alpha = 1.7$ and a distance of 780 kpc). For full details on source counts and background extraction and events corrections we refer to Fabbiano (1988).

2.1.2. ROSAT Data

For the energy spectra of Bo 375, we only analyzed only long (> 20 ksec) observations. There are three long observations in the archival database, and two of them (*ROSAT*#2 and *ROSAT*#3) are just outside the 'rib' support structure at $18'$ from the center of the field. The remaining one (*ROSAT*#1) is $\sim 14'$ off-axis. Each spectrum was extracted from a circular aperture centered on the source. The size of the extraction radius varied from $7''$ to $9''$ with the off-axis angle of the source to account for the point-spread function of the instrument. Background was subtracted from an annulus centered on the source. The spectra were binned so that there are at least 20 photons in each energy bin, and all channels below 0.1 keV and above 2.4 keV were ignored.

2.1.3. ASCA Data

The *Advanced Satellite for Cosmology and Astrophysics* (*ASCA*) satellite (Tanaka et al. 1994) is equipped with two Solid State Imaging Spectrometers (SIS; 0.4–10 keV) and two Gas Imaging Spectrometers (GIS; 0.7–10 keV). For our purpose, we only used the data taken by GIS instruments, because the source was near the edge of SIS. *ASCA* observed Bo 375 on 1993 July 29. Standard data screening was employed¹. Data taken at a geomagnetic cut-off rigidity lower than 4 GeV, at an elevation angle less than 5° from the Earth's limb, and during passage through the South Atlantic Anomaly were rejected. After filtering, the total net exposure time of each GIS was 16.2 ksec. We extracted the GIS spectra from a circular region of radius $6'$ centered at the position of the source, while the background was extracted from an annulus region around the source. Spectra were rebinned to have at least 20 photons in each energy bin and we fitted the GIS2 and GIS3 spectra simultaneously. We also set the normalization of GIS3 to be a

¹See the *ASCA* Data Reduction Guide 2.0 (<http://heasarc.gsfc.nasa.gov/docs/asca/abc/abc.html>)

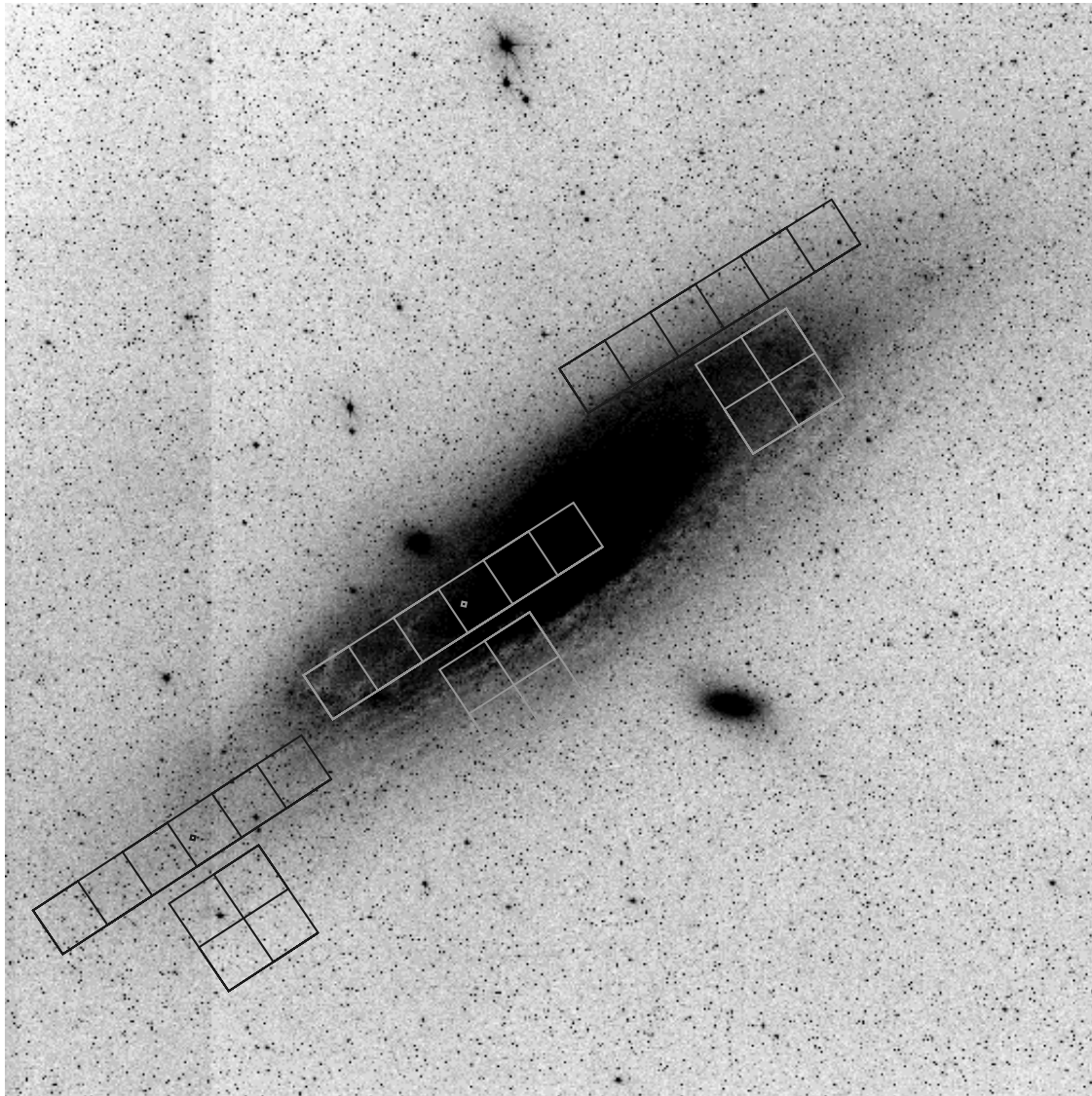


FIG. 1.— The regions observed by the M31 AO2 GO census. The chip orientation is shown for the 15 ksec observations that occurred in November 2000. Subsequent observations have (or will be) rotated by 90° and then a further 120° . Each aim-point (always in S3) is marked by a black, white or gray diamond (\diamond).

TABLE 1
OBSERVATION LOG OF Bo 375

Date	Observatory	Instrument	Exposure (ksec)	Count rate (c/s)	Remarks
7 August 1979	<i>Einstein</i>	HRI	9.9	0.03	
25 July 1991	<i>ROSAT</i>	PSPC	30.2	0.20	<i>ROSAT</i> #1
26 July 1991	<i>ROSAT</i>	PSPC	26.6	0.20	<i>ROSAT</i> #2, near the ‘rib’
5 January 1991	<i>ROSAT</i>	PSPC	44.7	0.11	<i>ROSAT</i> #3, near the ‘rib’
29 July 1993	<i>ASCA</i>	GIS	32.4	0.09	
30 November 1999	<i>Chandra</i>	HRC	1.2	0.19	
13 February 2000	<i>Chandra</i>	HRC	0.8	0.27	
8 March 2000	<i>Chandra</i>	HRC	2.1	0.25	
26 May 2000	<i>Chandra</i>	HRC	1.2	0.23	
21 June 2000	<i>Chandra</i>	HRC	1.2	0.31	
18 August 2000	<i>Chandra</i>	HRC	1.2	0.26	
11 September 2000	<i>Chandra</i>	HRC	1.2	0.21	
12 October 2000	<i>Chandra</i>	HRC	1.2	0.30	
1 November 2000	<i>Chandra</i>	ACIS-S	13.8	0.60	
1 February 2001	<i>Chandra</i>	HRC	1.2	0.23	

NOTES — This list includes only those observations we have used in this paper.

free parameter to account the difference in the calibration of the two detectors. In all fits the GIS3 normalization relative to GIS2 is about 5%.

2.1.4. *Chandra* Data

Bo 375 was located in the field of an ongoing (GO–AO2) X-ray census of M31. It was observed on 2000 November 1 for 15 ksec. The Advanced CCD Imaging Spectrometer (ACIS-S) was in the focal plane and Bo 375 was located in the ACIS-S2 chip and was $\sim 4.4'$ from the aim-point. Data were extracted from 0.3–7 keV to minimize the background, and a circular extraction region of radius 6" centered at the source position was used. Background was also extracted from an annulus region centered on the source and it contributed less than 0.1%. The source spectrum was rebinned so that there are at least 20 photons in each energy bin in order to allow χ^2 statistics. The response matrix and the ancillary response file were generated by CIAO v2.1². We note that the *Chandra* spectrum suffers significant pile-up ($\sim 30\%$).

In addition, a sequence of short (0.8 ksec to 2 ksec [see Table 1]) High Resolution Camera (HRC) exposures was available, because Bo 375 happened to be imaged during more than one year of monitoring carried out as part of a GTO program (see Garcia et al. 2000). In these images, Bo 375 was $\sim 10'$ off-axis. We have extracted the light curve of the source from a 25" circular region centered on the source position.

2.2. Analysis and Results

The spectra for the *ROSAT* *ASCA* and *Chandra* data were fitted with a variety of spectral models using XSPEC v11³. We first tried to fit the spectra with single-component models including absorbed power-law, black-body, thermal bremsstrahlung, disk black-body and cut-off power-law models. Power-law models provide good fits to each data set, except the *Chandra* ACIS-S data. Derived values of photon index range from 1.3 to 1.7, with $N_H \sim (1-3) \times 10^{21} \text{ cm}^{-2}$. The Galactic hydrogen column in the direction of M31 is about $7 \times 10^{20} \text{ cm}^{-2}$ (Dickey & Lockman 1990), and therefore our results are consistent with additional local absorption, either due to M31 itself or to absorption within the system. An absorbed black-body model gave a value of N_H ($\sim 3 \times 10^{20} \text{ cm}^{-2}$) smaller than the Galactic value for all observations, and we therefore discarded this model. We also fit the data to

thermal bremsstrahlung, cut-off power-law, and disk black-body models; these fits gave very large uncertainties for the *ROSAT* and *ASCA* data, and the fit was unacceptable ($\chi^2_\nu \sim 1.4$) for the *Chandra* data. Results of spectral fits to single-component models are shown in Table 2. The errors correspond to 90% confidence levels for a single interesting parameter.

We next tried to fit the spectra with different two-component models. A black-body plus power-law model gave an acceptable fit ($\chi^2_\nu = 1.27$) for the *Chandra* data; for the *ASCA* data, the additional black-body component does not improve the fit significantly (at the 99% level), indicating that the black-body component is soft ($< 1 \text{ keV}$). To check the fit of the *Chandra* data, we also fitted the *ROSAT* and *ASCA* data simultaneously so that we have broad energy coverage from 0.1–10 keV. Since Bo 375 is a variable, we choose the *ROSAT* observation with flux level similar to that of the *ASCA* data. The 0.5–2.4 keV fluxes of *ROSAT*#1 and *ROSAT*#2 were $\sim 4\%$ lower than the *ASCA* observation. *ROSAT*#2 is close to the ‘rib’ and there are shadowing effects. We therefore used *ROSAT*#1 for the joint spectral fittings. A single power-law model gave a reasonable fit to the data, and a black-body plus power-law model did improve the fit ($\chi^2_\nu = 1.16$). We replaced the power-law component with a cut-off power law. However, it did not give a better fit and the cut-off energy is larger than 10 keV, indicating that the cut-off energy is much higher than 10 keV and is therefore not accessible to either *ASCA* or *Chandra*.

Note that the spectral fit to the *Chandra* data may be affected by pile-up, which we have estimated to be at the 30% level. Normally one would expect pile-up to yield a somewhat harder spectrum than the true emitted spectrum. In fact, the values of α and kT derived from the *Chandra* data are in good agreement with those derived from the combined *ROSAT/ASCA* fit, which does not suffer from pile-up. The higher value of N_H in the *Chandra* fit may, however, be related to the effects of pile-up.

We also employed a disk black-body component instead of black-body, it gave a equally good fit ($\chi^2_\nu = 1.17$) but with larger errors on all parameters. The derived inner radius of the accretion disk $R_m \sqrt{\cos \theta}$ is $10 \pm 6.2 \text{ km}$ (assuming distance to M31 is 780 kpc; Stanek & Garanovich 1998) with the disk temperature of $1.95 \pm 0.35 \text{ keV}$. In Table 2, we have summarized the best-fit parameters.

Since the estimated metallicity of Bo 375 is low (6% solar; Huchra,

²<http://asc.harvard.edu/ciao/>

³<http://heasarc.gsfc.nasa.gov/docs/xanadu/xspec/index.html>

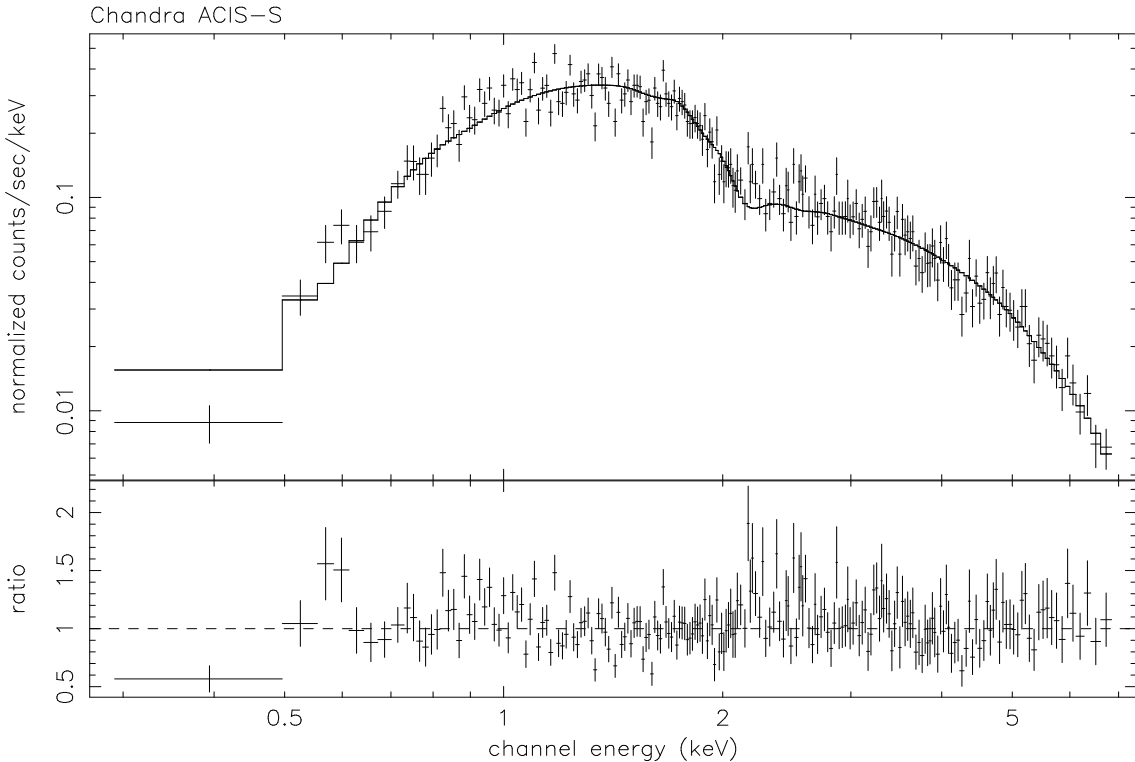


FIG. 2.— *Chandra* ACIS-S spectral fit of Bo 375. The spectrum was fitted by an absorbed power law plus blackbody model ($N_H = 3.35 \times 10^{21} \text{ cm}^{-2}$, $\alpha = 1.67$ and $kT = 0.80 \text{ keV}$) The observed luminosity (0.3–7 keV) at 780 kpc is $4.2 \times 10^{38} \text{ ergs s}^{-1}$.

Brodie & Kent 1991), we employed a photoelectric model with variable abundances (VPHABS in XSPEC), together with a photoelectric absorption fixed at the value towards M31, $7 \times 10^{20} \text{ cm}^{-2}$. We grouped H and He as one parameter fixed at the cosmic value, and set other metals (C, N, O, Ne, Na, Mg, Al, Si, S, Cl, Ar, Ca, Cr, Fe, Ni, and Co) as another parameter, fixing the abundance at 0.06 of the solar value. The black-body plus power-law model of the *Chandra* data was improved ($\chi^2_{\nu} = 1.29/206 \text{ dof}$; $N_{H,\text{vphabs}} = (4.33 \pm 0.67) \times 10^{21} \text{ cm}^{-2}$; $\alpha = 1.39 \pm 0.10$; $kT = 0.76 \pm 0.05 \text{ keV}$). However, there is no improvement on the joint *ROSAT* and *ASCA* data and the parameters are roughly the same as before.

2.3. Discussion

We have performed spectral analysis of Bo 375 using extensive *ROSAT* *ASCA* and *Chandra* data. The spectral characteristics resemble those seen in low-mass X-ray binaries (LMXBs). The source spectra can be well fitted by a single power-law. However, for data which span the widest range of energies, combined *ROSAT* and *ASCA* data and recent *Chandra* observations, an additional black-body component improves the fit. Such a two-component model was previously used to study the spectrum of many LMXBs including GC sources X 2127+119, X 1746–370 and X 1724–308 (e.g. Christian & Swank 1997; Guainazzi et al. 1998; Church & Balucinska-Church 2001) in our Galaxy. Our derived photon index and black-body temperature for Bo 375 are about 1.6 and 0.8 respectively, which is similar to that of X 2127+119 (Christian et al. 1997) and X 1724–308 (Guainazzi et al. 1998).

There are several possible physical explanations for the spectral model. The soft thermal component (i.e. black-body component) could originate from either an optically thick accretion disk or an optically thick boundary layer where the accreted matter interacts with the neutron star surface (see, e.g. White, Stella & Parmar 1988). The power-law component can be formed by scattering of the soft black-body photons in an extended region above the accretion disk, or from an optically thin boundary layer (Guainazzi et al. 1998; Barret et al. 2000).

2.4. Why is Bo 375 so luminous?

The spectral fits tell us that the luminosity of Bo 375 has ranged from $\sim 2-6 \times 10^{38} \text{ ergs s}^{-1}$ during the past 20 years. This makes it more luminous than any Galactic GC source by a factor that can be larger than 10. The source is also more luminous than the other GC sources we have so far studied in M31, but by a much smaller factor (approximately a factor of 2).

2.4.1. Is Bo 375 an unusual globular clusters?

Bo 375 (also known as G307) is not an unusual M31 globular cluster. The values of its measured parameters are very close to the median values for M31's globular cluster system: $V = 17.62$ (17.04 is the median value); $B-V = 0.90$ (0.90 is the median value); $V-R = 0.54$ (0.56 is the median value); $V-I = 1.02$ (1.20 is the median value); Its radial velocity is $-196 \pm 70 \text{ km/s}$, while -280 km/s is the median value. $[\text{Fe}/\text{H}] = -1.23 \pm 0.22$, with -1.21 the median value. Thus, aside from being a bit fainter and having a somewhat less negative radial velocity, Bo 375 is incredibly typical. In a coordinate system centered on M31, with X equal to the distance along major axis and Y equal to the distance along minor axis, it's at $X = 40'$, $Y = -12'$; i.e., it is projected just inside the disk boundaries.

It is also important to compare its properties to those of the Galactic globular clusters that house X-ray sources. A key parameter is metallicity, since metallicity effects can effectively alter the Eddington limit. Since $[\text{Fe}/\text{H}]$ for Galactic globular clusters with bright X-ray sources ranges from -0.28 to -2.25 , with $-1.22 < [\text{Fe}/\text{H}] < -0.96$ for 3 clusters with bright sources, Bo 375, the metallicity of Bo 375 seems unlikely to be the culprit that makes its X-ray emission so bright.

2.4.2. Is it a Multiple Source?

We will argue in §6 that multiple X-ray sources are expected among the M31 globular clusters. Thus, the most natural explanation for a high-luminosity source in an M31 globular cluster may be that the source is actually a composite of 2 or more sources. We have therefore

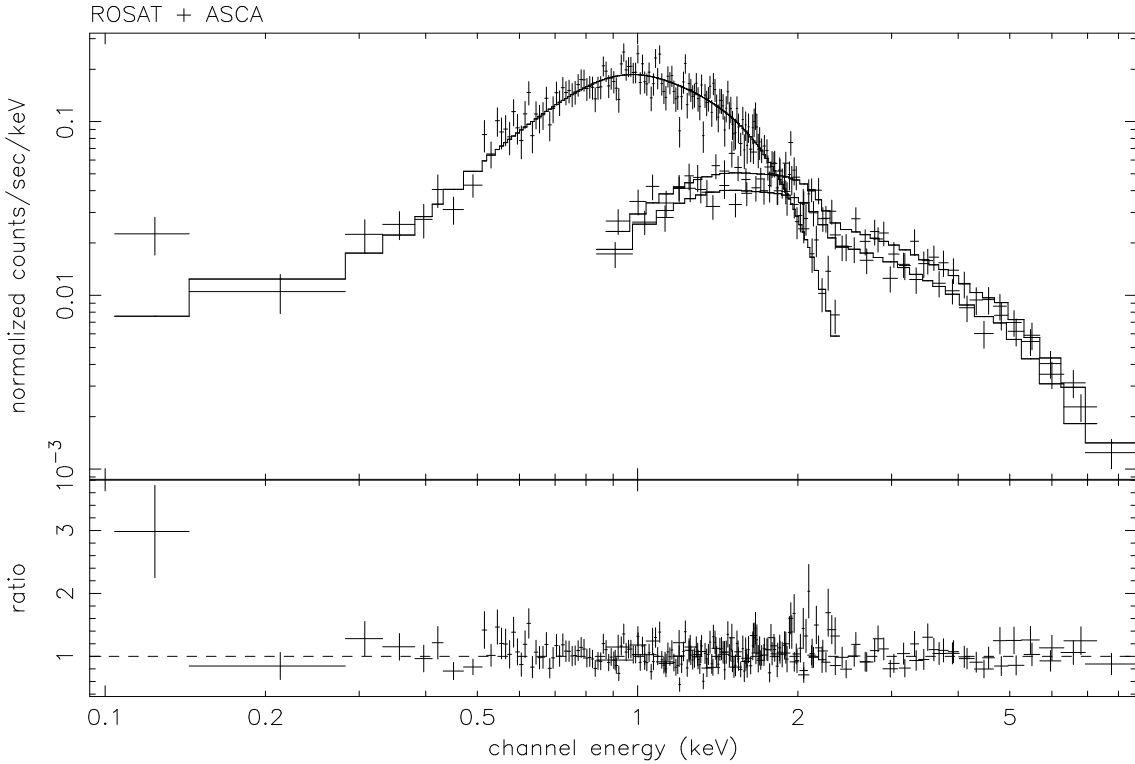


FIG. 3.— Joint *ROSAT* and *ASCA* spectral fit of Bo 375. The spectrum was fitted by an absorbed power law plus blackbody model ($N_H = 1.61 \times 10^{21} \text{ cm}^{-2}$, $\alpha = 1.61$ and $kT = 0.86 \text{ keV}$) The observed luminosity (0.3–7 keV) at 780 kpc is $6.1 \times 10^{38} \text{ ergs s}^{-1}$.

TABLE 2
BEST-FIT PARAMETERS FOR THE ENERGY SPECTRA OF BO 375

Observation	N_H (10^{21} cm^{-2})	α	kT ^a (keV)	$R_{in} \sqrt{\cos \theta}$ ^b (km)	χ^2_{ν}/dof	Luminosity ^c
<i>ROSAT</i> #1	0.96 ± 0.96	1.33 ± 0.08			1.32/156	2.16
<i>ROSAT</i> #2	0.98 ± 0.15	1.30 ± 0.11			1.01/147	2.34
<i>ROSAT</i> #3	1.10 ± 0.20	1.32 ± 0.12			0.90/148	1.43
<i>ASCA</i>	2.20 ± 0.60	1.70 ± 0.07			0.90/81	2.25
<i>Chandra</i>	3.91 ± 0.16	1.67 ± 0.03			1.53/209	1.42
	3.35 ± 0.34	1.67 ± 0.13	0.80 ± 0.11		1.40/207	1.44
<i>ROSAT</i> #1+ <i>ASCA</i>	1.20 ± 0.90	1.58 ± 0.04			1.22/238	2.29
	1.61 ± 0.08	1.61 ± 0.08	0.86 ± 0.12		1.16/236	2.29
	1.10 ± 0.20	1.77 ± 0.34	1.95 ± 0.35	10 ± 6.2	1.17/236	2.28

NOTES — The power-law model is defined as $AE^{-\alpha}$, where A is the normalization at 1 keV (photons $\text{cm}^{-2} \text{ s}^{-1} \text{ keV}^{-1}$) and E is in keV.

^a Black-body temperature or inner disk temperature

^b Assuming a distance of 780 kpc

^c Emitted 0.5–2.4 keV luminosity in units of $10^{38} \text{ erg s}^{-1}$; we choose this energy range for convenient comparison with *ROSAT* data.

studied the image (composed of hits by ~ 7000 photons) of Bo 375 to see if it suggests multiplicity. Indeed, the image breaks into 2 components, but we find that this is most likely due to the shape of the point spread function (PSF) at the position of the source. Nevertheless, there appears to be some residual broadening of the image along the direction perpendicular to the PSF-induced binarity. Further checks of the PSF, especially attuned to the spectrum of Bo 375, are necessary to establish that the broadening is a real effect. While such work is underway, we note that the maximum separation between components consistent with our observations is $\sim 1\text{--}2''$, which corresponds to a physical projected separation of $\sim 3.7\text{--}7.4$ pc. Such a separation could be consistent with a model in which there are two or three X-ray bright binaries in the cluster, and one or two of these binaries was ejected from the cluster core $\sim 10^5$ years ago. Such separations, and even smaller ones, could be resolved by an on-axis observation with the HRC. Depending on the nature of the sources, HST measurements could also prove to be valuable.

The ejection of X-ray binaries from the core of a globular cluster, achieving \sim pc separations while the X-ray evolution continues, is consistent with physical models of X-ray sources in globular clusters. The basic picture that has emerged to explain the overabundance (by a factor of ~ 100 ; Clark 1975) of X-ray sources in globular clusters, is the following. Stars with the highest masses, and also primordial binaries, migrate toward the cluster centers. Stellar densities near the center are typically so high ($10^3\text{--}10^6$ stars pc $^{-3}$) that individual stars and binaries can interact via two-body, three-body (2 + 1) and four-body (2 + 2) interactions. Such interactions can produce close binary systems which subsequently experience mass transfer and are luminous at X-ray wavelengths. These close binaries store a great deal of potential energy; if they interact with other stars or binary systems, they (or the systems with which they have interacted) can be ejected from the core and even from the globular cluster. Thus the environment that favors the formation of X-ray binaries in or near the cores of globular clusters also leads them to eventually be ejected from the cores or even from the clusters.

For Bo 375, however, multiplicity is likely to be, at most, only part of the story. As described in §2.4.3, there is significant time variability over timescales ranging from 16 hrs to many months; this indicates that one source must contribute a large fraction (although possibly not all) of the detected flux.

2.4.3. Is it a Black Hole?

When observing a source which is more luminous than the Eddington limit for a $1.4M_{\odot}$ object, it is natural to conjecture that the accreting source may be a black hole. Reliable detections of solar-mass black holes have so far been based on orbital studies that find upper limits on the mass of an accreting compact object well above the maximum mass predicted for neutron stars (see, e.g., Charles 1998). Such a study is not presently feasible for Bo 375. We must therefore search for spectral signatures that could possibly distinguish between neutron star and black hole models. First-principles calculations and comparisons between the spectra of neutron star accretors and dynamically-confirmed black hole accretors can provide some insight. No reliable set of tests is presently available, however, to allow us to place Bo 375 firmly in either the “black hole” or “neutron star” camp.

The discussion at the end on §2.3 indicates that there are similarities between the spectra of MW GC X-ray sources, which are known to be accreting neutron stars, and the spectrum of Bo 375. Such broad similarities are, however, only suggestive and cannot definitively establish the nature of the source.

The time variability (discussed below) may also indicate that nature of the accreting object. While Bo 375 is highly variable, it is not a transient source. Within the MW, black hole binaries can be separated into those that are transient, and those that are persistent. The persistent sources have high mass secondaries (generally above $5M_{\odot}$), while the transient systems tend to have low mass secondaries (see Tanaka & Shibasaki 1996, Table 2). Given the location of this source in a GC, the secondary is likely to be of low mass. Its non-transient nature

and likely low-mass secondary could then be taken to argue against the black hole hypothesis. However, we add the following caveat to this argument. The transient nature of the systems with low mass secondaries is likely caused by mass transfer rates which are below a critical value for stability (van Paradijs 1996). Even low mass secondaries can briefly supply high mass transfer rates when they begin moving off the main sequence (see section 6.1 herein). Should Bo 375 be in this unusual state, its persistent nature would not indicate the nature of the primary.

2.4.4. Time Variability

The neutron-star nature of the MW GC X-ray sources was definitively established by observations of time variability. Specifically, X-ray bursts have been observed from all globular cluster X-ray sources. These bursts can be linked to the episodic nuclear burning of matter accreted by the neutron star. An X-ray source can also be established as a neutron star system if it is observed to emit periodic X-ray pulses.

Given the important role time variability studies have played in helping us to understand Galactic GC X-ray sources, it is important to study the time variability of Bo 375. We have used the GO data set to study its short-term behavior. (Note that the count rate (~ 0.5 counts/s) is too low to allow us to probe time scales much shorter than a minute.) Fourier analysis does not find evidence of periodicity, and there is no evidence of bursts. Thus, the light curve does not allow us to establish that all or part of the X-radiation is emitted by a neutron star system.

In Figure 4 we show the light curves of data binned into intervals of 0.5 min, 1 min, 5 min, and 10 min. Data from Bo 375 is displayed on the left. Let A_{ti} be the average number of counts in the time interval under consideration. The upper (lower) dashed line is positioned at $A_{ti} + \sqrt{A_{ti}}$ ($A_{ti} - \sqrt{A_{ti}}$) These two dashed lines thus provide guidelines to the uncertainty due to the counting statistics. The dark uneven curve that generally lies between these two dashed lines is the running average, computed by considering the central bin and the four previous and subsequent bins. At short time scales, there is no evidence for time variability.

The light curves plotted on the right are also taken from the Bo 375 data, but the order of the data points (taken in 5 s time bins) has been randomized. There are no readily quantifiable differences between the randomized and correctly-time-ordered data.

Whereas these observations covered a time interval of roughly 4 hours, the 1991 *ROSAT* survey of M31 has data on Bo 375 that spans a baseline that is roughly 10 times longer. Supper et al. (1997) find evidence for regular variations of $\sim 50\%$ on a time scale of ~ 16 hours. Proceeding to longer time scales, Bo 375 was in the fields visited at regular (\sim monthly) intervals by *Chandra*’s HRC for ~ 1 ksec observations. This data set also finds significant variations from 50–100% (Figure 6).

In summary, what we know so far about Bo 375’s time variability provides no hint that the X-ray source is a neutron star. The data do suggest, however, that if the Bo 375 source is a multiple, the number of separate bright components is small. This implies that there is at least one X-ray binary whose luminosity appears to be comparable to the Eddington limit for a $1.4M_{\odot}$ accretor. We find that a model in which the luminosity is generated by mass transfer onto a neutron star, occurring on the thermal time scale of the donor, is consistent with this data (§6). Alternatively, the high luminosity could be an effect of beaming, or it could be associated with a high-mass, possibly a black hole, accretor.

3. OTHER BRIGHT M31 GC SOURCES

3.1. Brief Description of Data

Our *Chandra* census fields (see Figure 1) contained other bright X-ray sources also in GCs. This suggested that it would be valuable to include additional M31 fields which had already been observed by *Chandra*. Such data was collected by a GTO program (see Garcia et al. 2000; Primini et al. 2000). There were seven ACIS-I pointings of

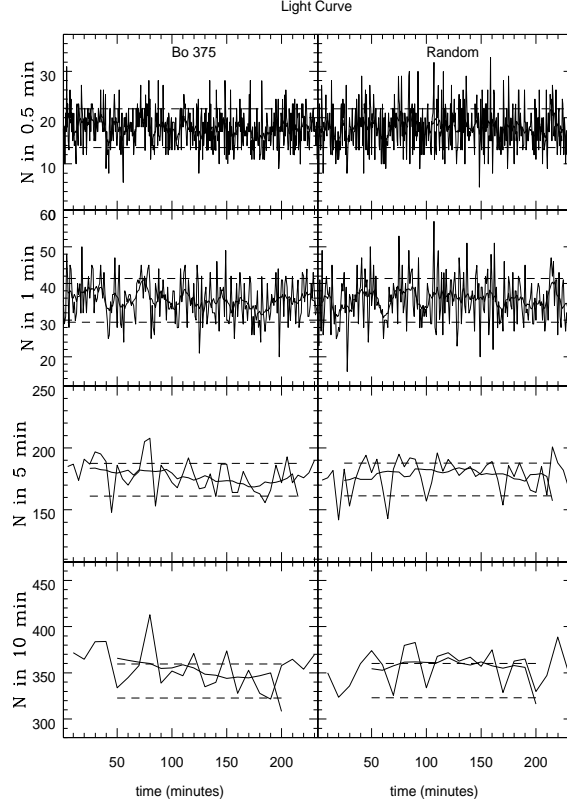


FIG. 4.— The light curves of Bo 375 binned into intervals of 0.5 min, 1 min, 5 min and 10 min. See §2.4.4 for discussion.

the central $16' \times 16'$ region around the galaxy from 1999-2000. For the analysis below, we used 8.8 ksec from the longest pointing (1999 October 13), except that two additional GCs were observed on 1999 December 11 and 2000 January 29.

3.2. The Sources

Table 3 provides a complete list of all of the X-ray sources we have observed in M31 globular clusters. The sources are listed in order of count rate; the source with the highest count rate appears first. For each source, the coordinates (J2000), optical ID and luminosity (assuming a power law model with $N_H = 10^{21} \text{ cm}^{-2}$ and photon index $\alpha = 1.7$) are included. Three sources (Source 2, 13 and 15) have been observed by two GO pointings and we list both observations with the first one corresponding to the earlier observations. Table 4 lists the counts in a sequence of energy bins.

Optical IDs: A wavelet detection algorithm (WAVDETECT in CIAO) was used to find X-ray sources. Each *Chandra* source was placed at the center of a $3''$ source region. We cross-correlated with catalogs of globular clusters (Battistini et al. 1987; Magnier 1993; Barmby et al. 2000; Barmby 2001). Typical offsets between the globular clusters and our X-ray sources are about $1''$; when a cluster appears in multiple catalogs, the offsets may differ somewhat.

3.3. Hardness Ratios and Spectra

In order to quantify the spectral behavior of M31 X-ray GCs, we complied a table for the counts in different energy bins (see Table 4). The bins we use are $0.1 - 0.4$, $0.5 - 0.9$, $0.9 - 1.5$, $1.5 - 2.0$, $2 - 4$, and $4 - 10$ keV, respectively. The choice of ranges for the low-energy bins is based on the *ROSAT* bins typically used for these data sets (Verbunt et al. 1995, Supper et al. 1997), so as to facilitate comparisons between *Chandra* and *ROSAT* data sets. The count rates in each bin are background subtracted.

We implemented a set of spectral fits for each source with more than ~ 400 counts (0.3–7 keV). There are 4 such sources (in addition to Bo 375) and a total of 5 observations with such count rates. They are: Bo 82 with 3053 counts in the first GO pointing and 2277 counts in the second pointing, Bo 153 with 962 counts in a GTO pointing with ACIS-I, Bo 86 with 542 counts (also in a GTO pointing with ACIS-I), and Bo 143 with 446 counts.

We first tried to fit the spectra with a power law model with the hydrogen column density N_H as a free parameter. If the derived N_H was inconsistent with the observed color excess $E(B-V)$ from optical observations, then we fixed the N_H according to the optical absorption. We also tried to fit the spectra with other single component models such as blackbody and thermal bremsstrahlung model. All of the fits were either unacceptable ($\chi^2_\nu > 2$), or also the best-fit parameters were unrealistic. Finally, we fitted the spectra with power law plus blackbody models. Although these generally gave good fits, the blackbody temperature became unrealistic and the fits were not improved significantly. We describe below the best fit parameters of power law models.

Bo 82 – A power law model provided a good fit ($\chi^2_\nu = 1.03/114$ dof) for the first GO observation with $N_H = (5.17 \pm 0.31) \times 10^{21} \text{ cm}^{-2}$ and $\alpha = 1.42 \pm 0.06$. The emitting luminosity in 0.3–7 keV is $1.70 \times 10^{38} \text{ erg s}^{-1}$. For the second GO observation, we obtained $N_H = (4.58 \pm 0.40) \times 10^{21} \text{ cm}^{-2}$ and $\alpha = 1.14 \pm 0.07$, with $\chi^2_\nu = 1.16/88$ dof. The luminosity is $2.20 \times 10^{38} \text{ erg s}^{-1}$.

Bo 153 – The best fit parameters were $N_H = (1.07 \pm 0.33) \times 10^{21} \text{ cm}^{-2}$ and $\alpha = 1.38 \pm 0.10$, with $\chi^2_\nu = 0.92/40$ dof. The luminosity in 0.3–7 keV is $9.12 \times 10^{37} \text{ erg s}^{-1}$. Fixing the hydrogen column density $N_H = 6 \times 10^{20} \text{ cm}^{-2}$ [$E(B-V) = 0.11$] gave $\alpha = 1.26 \pm 0.05$ with $\chi^2_\nu = 0.96/41$ dof.

Bo 86 – Leaving the column density as a free parameter, a power law model provided a good fit with $\chi^2_\nu = 1.05/22$ dof. The best-fit parameters were $N_H = (1.28 \pm 0.50) \times 10^{21} \text{ cm}^{-2}$ and $\alpha = 1.37 \pm 0.15$. The

TABLE 3
GLOBULAR CLUSTER X-RAY SOURCES IN M31

ID	Source Name	R.A. (h:m:s)	Dec. (° :':")	Exposure (ksec)	$L_X(0.3-7 \text{ keV})$ ($10^{37} \text{ erg s}^{-1}$)	Optical ID
1 [†]	CXOU J004545.4+413942	00:45:45.431	+41:39:42.41	13.8	29.94	Bo 375, mita468
2 ^{†◊}	CXOU J004215.8+410114	00:42:15.899	+41:01:14.44	14.5	11.97	Bo 82, mita159
				13.0	8.90	
3 [†]	CXOU J004310.6+411450	00:43:10.647	+41:14:50.50	8.8	8.43	Bo 153, mita251
4 [†]	CXOU J004218.5+411400	00:42:18.598	+41:14:00.63	8.8	4.69	Bo 86, mita164
5 [†]	CXOU J004259.6+411918	00:42:59.655	+41:19:18.67	8.8	2.79	Bo 143
6	CXOU J004259.8+411604	00:42:59.867	+41:16:04.96	8.8	2.68	Bo 144
7 [†]	CXOU J004302.9+411521	00:43:02.940	+41:15:21.77	8.8	2.18	Bo 146
8 [†]	CXOU J004303.8+411804	00:43:03.872	+41:18:04.17	8.8	1.83	Bo 148
9 [†]	CXOU J004337.3+411442	00:43:37.328	+41:14:42.42	4.1	1.83	mita299
10	CXOU J004209.4+411744	00:42:09.438	+41:17:44.52	8.8	1.17	mita140
11 [†]	CXOU J004303.2+412121	00:43:03.291	+41:21:21.41	8.8	1.09	Bo 147, mita240
12 [†]	CXOU J004314.4+410726	00:43:14.417	+41:07:26.27	4.1	0.91	Bo 158
13 ^{†◊}	CXOU J004206.1+410248	00:42:06.180	+41:02:48.29	14.5	0.85	Bo D42, mita130
				13.0	0.74	
14	CXOU J004226.0+411914	00:42:26.007	+41:19:14.26	8.8	0.74	Bo 96, mita174
15 [◊]	CXOU J004207.1+410016	00:42:07.180	+41:00:16.54	14.5	0.71	Bo D44
				13.0	0.31	
16 [†]	CXOU J004231.2+411938	00:42:31.223	+41:19:38.23	8.8	0.44	Bo 107, mita192
17	CXOU J004246.0+411735	00:42:46.054	+41:17:35.30	8.8	0.31	PB-in7 [♣]
18	CXOU J004240.6+411031	00:42:40.676	+41:10:31.70	8.8	0.28	Bo 123, mita212
19	CXOU J004307.5+412019	00:43:07.531	+41:20:19.01	8.8	0.27	Bo 150, mita246
20	CXOU J004212.0+411757	00:42:12.098	+41:17:57.87	8.8	0.26	Bo 78, mita153
21 [†]	CXOU J004225.0+405719	00:42:25.041	+40:57:19.13	13.0	0.17	Bo 94, mita173
22	CXOU J004255.6+411834	00:42:55.609	+41:18:34.41	8.8	0.17	Bo 138
23	CXOU J004152.9+404710	00:41:52.973	+40:47:10.64	13.0	0.13	Bo 58, mita106
24	CXOU J004241.4+411522	00:42:41.423	+41:15:22.86	8.8	0.11	mita213
25 [*]	CXOU J004219.6+412153	00:42:19.644	+41:21:53.22	8.8	0.08	mita165, mita166
26	CXOU J004227.4+405936	00:42:27.457	+40:59:36.17	13.0	0.08	Bo 98
27	CXOU J004315.4+411124	00:43:15.488	+41:11:24.09	8.8	0.06	Bo 161, mita260
28	CXOU J004141.0+410401	00:41:41.097	+41:04:01.53	13.0	0.06	mita87
29	CXOU J004250.7+411032	00:42:50.745	+41:10:32.24	8.8	0.05	mita222, PB-in2 [♣]
30	CXOU J004136.5+410017	00:41:36.567	+41:00:17.75	14.5	0.04	Bo 251

NOTES — Observations lasting longer than 10 ksec were carried out as part of the GO program (see Figure 1); Shorter observations around the central $16' \times 16'$ field were carried out as part of the GTO program (Garcia et al. 2000; Primini et al. 2000).

† Source detected by *ROSAT* (Supper et al. 1997)

◊ Source detected in both GO observations

♣ Results based on an HST survey (Barmby 2001)

* Source 25 is associated with two clusters: mita165 and mita166

TABLE 4
COUNTS IN DIFFERENT ENERGY BANDS OF GLOBULAR CLUSTER X-RAY SOURCES IN M31

Source	Counts						Hardness Ratio ^a
	0.1–0.4 keV	0.5–0.9 keV	0.9–1.5 keV	1.5–2 keV	2–4 keV	4–10 keV	
1	0.0 ± 0.0	593.8 ± 24.4	2319.1 ± 48.2	1509.0 ± 38.8	2060.8 ± 45.4	897.4 ± 30.1	1.0
2	9.3 ± 3.3	178.8 ± 13.4	817.7 ± 28.6	633.3 ± 25.1	993.6 ± 31.5	423.0 ± 20.7	1.4
	7.4 ± 3.1	135.4 ± 11.7	509.4 ± 22.7	461.9 ± 21.5	740.9 ± 27.3	425.4 ± 20.8	1.8
3	0.7 ± 1.0	121.8 ± 11.0	322.5 ± 18.0	163.3 ± 12.7	233.5 ± 15.3	123.3 ± 11.1	0.8
4	1.0 ± 1.0	66.3 ± 8.1	186.0 ± 13.6	104.3 ± 10.2	128.3 ± 11.3	57.4 ± 7.6	0.7
5	1.0 ± 1.0	54.4 ± 7.4	126.1 ± 11.2	52.9 ± 7.2	65.1 ± 8.1	21.7 ± 4.7	0.5
6	1.0 ± 1.0	35.8 ± 6.0	91.0 ± 9.5	58.6 ± 7.6	75.9 ± 8.7	44.5 ± 6.7	0.9
7	1.0 ± 1.0	36.7 ± 6.0	88.0 ± 9.3	48.4 ± 6.9	59.1 ± 7.7	20.8 ± 4.5	0.6
8	1.0 ± 1.0	29.7 ± 5.4	87.7 ± 9.3	43.8 ± 6.6	32.0 ± 5.6	14.7 ± 3.8	0.4
9	1.0 ± 1.0	8.2 ± 3.3	33.8 ± 5.9	11.3 ± 3.7	27.3 ± 5.4	14.1 ± 4.3	1.0
10	0.0 ± 0.0	8.0 ± 2.8	56.9 ± 7.6	30.5 ± 5.5	28.1 ± 5.3	12.3 ± 3.5	0.6
11	0.0 ± 0.0	24.0 ± 4.8	56.3 ± 7.5	16.3 ± 4.0	20.2 ± 4.5	9.3 ± 3.1	0.3
12	0.0 ± 0.0	1.0 ± 1.0	8.0 ± 2.8	6 ± 2.4	22.0 ± 4.8	10.5 ± 3.3	3.6
13	11.0 ± 3.4	74.3 ± 8.6	83.3 ± 9.1	26.6 ± 5.1	30.2 ± 5.5	5.0 ± 3.0	0.2
	5.4 ± 2.4	52.7 ± 7.2	65.4 ± 8.1	23.0 ± 4.7	25.7 ± 5.1	8.2 ± 3.0	0.3
14	0.0 ± 0.0	11.0 ± 3.3	37.5 ± 6.1	15.8 ± 3.9	14.9 ± 3.8	7.0 ± 2.6	0.4
15	1.0 ± 1.4	24.3 ± 5.0	65.3 ± 8.1	35.6 ± 6.0	40.2 ± 6.4	20.0 ± 4.9	0.6
	0.0 ± 0.0	16.7 ± 4.1	21.0 ± 4.5	13.0 ± 3.6	18.0 ± 4.2	9.2 ± 3.1	0.7
16	0.0 ± 0.0	10.3 ± 3.2	15.7 ± 4.0	10.4 ± 3.2	12.3 ± 3.6	2.7 ± 1.7	0.6
17	0.0 ± 0.0	1.8 ± 1.4	14.5 ± 3.8	3.8 ± 2.0	13.0 ± 3.6	2.6 ± 1.7	0.9
18	0.0 ± 0.0	4.7 ± 2.2	14.0 ± 3.7	3.7 ± 2.0	4.9 ± 2.3	6.1 ± 2.5	0.6
19	0.0 ± 0.0	6.0 ± 2.4	13.5 ± 3.8	6.0 ± 2.4	5.1 ± 2.3	2.0 ± 1.4	0.4
20	0.0 ± 0.0	2.0 ± 1.4	5.5 ± 2.4	8.0 ± 2.8	9.0 ± 3.2	3.0 ± 1.7	1.6
21	0.0 ± 0.0	6.0 ± 2.4	16.0 ± 4.0	7.0 ± 2.6	8.0 ± 2.8	5.2 ± 2.4	0.6
22	0.0 ± 0.0	6.0 ± 2.4	6.8 ± 2.6	3.8 ± 2.0	1.8 ± 1.4	1.8 ± 1.4	0.3
23	0.0 ± 0.0	0.5 ± 1.0	10.8 ± 3.7	5.1 ± 2.5	5.8 ± 2.9	10.1 ± 3.3	1.4
24	0.0 ± 0.0	0.0 ± 0.0	7.1 ± 2.8	2.0 ± 1.4	3 ± 1.7	1.4 ± 1.2	0.6
25	0.0 ± 0.0	0.0 ± 0.0	1.0 ± 1.9	0.0 ± 0.0	6.0 ± 2.4	3.0 ± 1.7	9.0
26	0.0 ± 0.0	2.7 ± 1.7	10.0 ± 3.1	4.0 ± 2.0	3.0 ± 1.7	0.4 ± 1.0	0.3
27	0.0 ± 0.0	1.5 ± 1.4	3.0 ± 2.1	3.0 ± 1.7	0.0 ± 0.0	0.1 ± 1.2	0.02
28	0.0 ± 0.0	0.5 ± 1.0	9.5 ± 3.1	3.1 ± 2.0	1.5 ± 1.4	0.5 ± 2.6	0.2
29	0.0 ± 0.0	2.8 ± 1.7	0.9 ± 1	0.0 ± 0.0	0.7 ± 1.0	2.0 ± 1.4	0.7
30	2.0 ± 1.4	5.4 ± 2.5	3.4 ± 2.0	0.0 ± 0.0	0.0 ± 0.0	0.8 ± 2.3	0.09

^a Hardness ratio is defined as 2–10 keV/0.5–1.5 keV

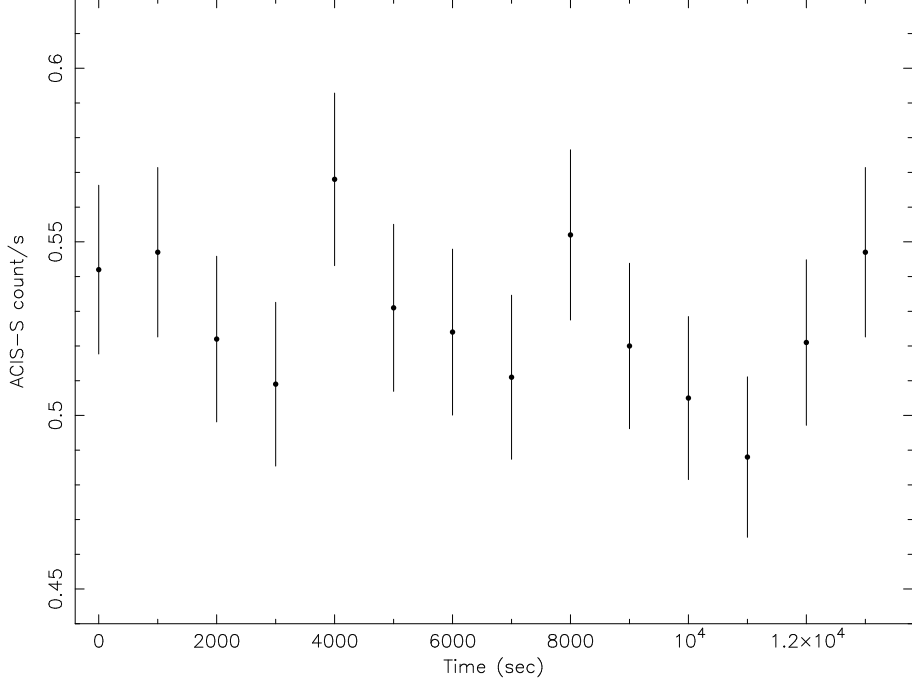


FIG. 5.— 15 ksec *Chandra* ACIS-S light curve of Bo 375. The time resolution is 1000 sec.

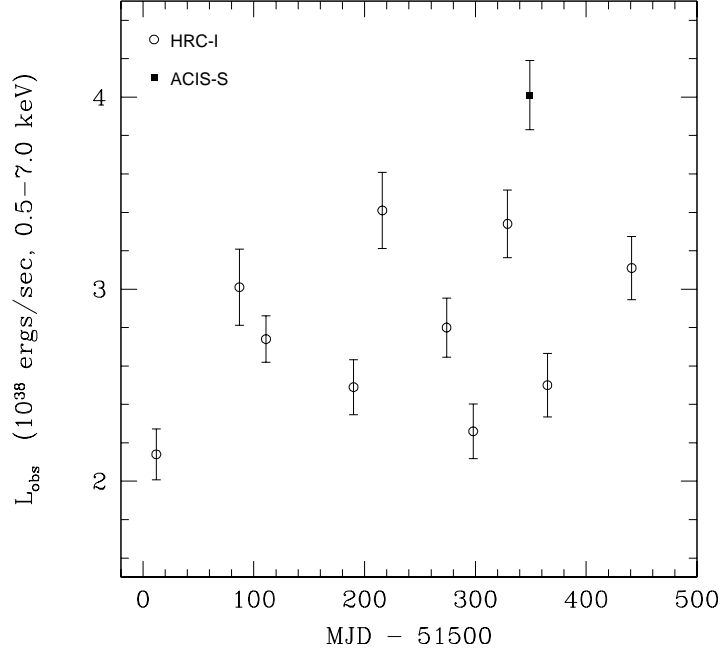


FIG. 6.— *Chandra* HRC light curve of Bo 375. The luminosity was estimated by PIMMS, using the observed count rate and assuming a power law spectral model with $N_H = 10^{21} \text{ cm}^{-2}$ and photon index $\alpha = 1.7$.

luminosity in 0.3–7 keV is $5.26 \times 10^{37} \text{ erg s}^{-1}$. We have fixed the absorption at $N_H = 4.4 \times 10^{20} \text{ cm}^{-2}$ [$E(B-V) = 0.08$] and we obtained $\alpha = 1.15 \pm 0.08$ with $\chi^2_{\nu} = 1.15/23$ dof.

Bo 143 — Power law is the only model which can be fitted for the

spectrum. We have obtained $N_H = (1.96 \pm 0.66) \times 10^{21} \text{ cm}^{-1}$ and $\alpha = 1.90 \pm 0.23$, with $\chi^2_{\nu} = 0.69/12$ dof. The luminosity in 0.3–7 keV is $3.17 \times 10^{37} \text{ erg s}^{-1}$. By fixing the absorption at $N_H = 7.2 \times 10^{20} \text{ cm}^{-2}$ [$E(B-V) = 0.13$], the best fit parameters were $\alpha = 1.50 \pm 0.10$ and

$$\chi^2_{\nu}=1.02/13 \text{ dof.}$$

Except for the second observation of Bo 82, the power-law photon index α ranges from 1.4 to 2 which is typical for low-mass X-ray binaries. For Bo 82, the photon index changed from 1.4 to 1.1, indicating a transition from a soft state to hard state but at a similar intensity level. Trinchieri et al. (1999) also found that Bo 82 to be a hard source and on that basis conjectured that it might be a black hole. *ROSAT* also observed Bo 82 (see Supper et al. 1997); we reanalyzed the archival data and a power-law with $\alpha \sim 1.4$ gave a good fit to the data.

We have constructed the time history of these four sources over ~ 500 days (see Figure 7). Just as for Bo 375, Bo 82 and Bo 86 show intensity variability by a factor of ~ 3 . In particular, Bo 86 may have long-term variability on timescales of ~ 200 days. Bo 153 and Bo 143 may be variable at a lower level but higher signal-to-noise light curves would be needed to establish variability.

4. POPULATION STUDIES

4.1. The Luminosity Function

Two types of information can be used to construct a luminosity function. First, of course, is the observed luminosities of the sources. This is the information we present in this paper, because our primary motivation is to feature the high-luminosity sources that have actually been detected and to compare the detected GC X-ray sources in M31 with detected GC X-ray sources in the Milky Way. It is also possible to take a more comprehensive view that takes into account the fact that we learn something about the luminosity function from computing upper limits for clusters which have been observed with X-ray detectors but within which no X-ray sources were discovered. Ongoing and possible new observations may extend the depth of M31 observations and their sensitivity to transient GC X-ray sources. Thus, a more complete picture of the M31 globular cluster X-ray sources is developing, and will warrant a later careful look at non-detections as well as detections.

In Figure 8 we present the luminosity distribution of all 30 GC X-ray sources observed by *Chandra*. Luminosities were derived assuming a power-law model with $N_H = 10^{21} \text{ cm}^{-2}$ and $\alpha = 1.7$ in 0.3–7 keV. The derived luminosities are not very sensitive to the spectral parameters; the difference is about 20% when varying the N_H from $6 - 15 \times 10^{22} \text{ cm}^{-2}$ and α from 1.2 to 2. The thermal Bremsstrahlung model used by Primini, Forman, & Jones (1993) gave luminosity differences up to 80%.

This luminosity function has 2 quantifiable differences with the Galactic GC X-ray luminosity function, even though the most recently published M31 GC luminosity function found the M31 and Galactic GC X-ray luminosity functions to be in agreement (Supper et al. 1997). First, the peak X-ray luminosity is higher by a factor of ~ 10 , and second, a larger fraction of all GC sources have luminosities above $10^{37} \text{ erg s}^{-1}$ ($\sim 10/30$ in M31, vs 1/12 in the Galaxy).

4.2. Previous Work

The discovery of high-luminosity sources in M31 X-ray sources began roughly 25 years ago. Twenty one X-ray sources discovered by instruments aboard the Einstein observatory were tentatively identified with globular clusters. The source identified with the cluster labeled by Sargent et al. (1977) as 307, which we have referred to as Bo 375, had a measured X-ray luminosity of $2.7 \times 10^{38} \text{ ergs s}^{-1}$. The source identified with Bo 135 had a measured X-ray luminosity of $1.1 \times 10^{38} \text{ ergs s}^{-1}$. Long & van Speybroek (1982), noted that these luminosities were higher than any observed for Galactic GCs. Battistini et al. (1987) further noted that the fraction of then-known M31 GCs with X-ray sources might also be larger than the fraction in our Galaxy. This was because, even though the measured fractions were similar, only the most luminous of the Galactic sources could have been detected in M31 by Einstein. This raised the question of whether the frequency of X-ray sources in M31 was generally higher, or whether the GC X-ray sources in M31 were brighter than Galactic GC sources. Observations of the central $\sim 34'$ of M31 with *ROSAT*'s HRI, discovered 18 GC X-ray sources and placed upper limits and placed upper limits on X-

ray detection from 32 additional globular clusters (Primini, Forman, & Jones 1993). All of the measured X-ray luminosities were below $10^{38} \text{ ergs s}^{-1}$, but 8 were above $10^{37} \text{ ergs s}^{-1}$. A statistical analysis, based on survival analysis techniques (Avni et al. 1980, Feigelson & Nelson 1985, Schmitt 1985) allowed the upper limits as well as the measured luminosities to be used to construct the luminosity function. This procedure produced a cumulative X-ray luminosity distribution that exhibited a maximum luminosity consistent with that of the Galactic GC X-ray luminosity distribution, but which seemed to have a larger population of high-luminosity sources. The most comprehensive survey to date is the 1991 *ROSAT* survey of M31, which detected 31 globular cluster X-ray sources (Supper et al. 1997; see also Supper et al. 2001). A statistical analysis that paralleled the one carried out by Primini et al. (1993) agreed that the maximum luminosity of M31 globular cluster sources is consistent with that of Galactic globular cluster sources. Based on this larger sample, however, it was concluded that there is no difference between the luminosity functions of M31 and Milky Way globular clusters.

Given the shifts in perception of the M31 GC luminosity function, we note that the higher-X-ray luminosities ($> 10^{38} \text{ erg s}^{-1}$) are well established in the *Chandra* data sets and in prior X-ray data. Overall, using PIMMS to convert measured count rates to X-ray luminosities for the power-law model used to construct the *Chandra*-measured luminosity function, we find that there are ~ 7 sources across data sets with X-ray luminosities near or above $10^{38} \text{ erg s}^{-1}$.

Even the result about the large fraction of sources with $L_x > 10^{37} \text{ erg s}^{-1}$ is likely to remain valid when additional observations of M31 GCs are carried out. To justify this statement, we first note that already-completed observations taken by other X-ray telescopes can be used to extend the *Chandra* sample, and that the extended samples exhibit this same characteristic. For example, the *ROSAT* data on 18 GC X-ray sources (Supper et al. 1997, 2001) that are not in our fields includes 6 GCs with $L_x[0.3-7 \text{ keV}]$ between 10^{36} and $10^{37} \text{ erg s}^{-1}$, and 12 GCs with $L_x[0.3-7 \text{ keV}] > 10^{37} \text{ erg s}^{-1}$. Second, we note that the only way for the fraction of sources with $L_x[0.3-7 \text{ keV}]$ to be reduced to the Galactic value would be if a very large number of M31 GCs were discovered to house lower-luminosity bright sources ($10^{35} < L_x < 10^{37} \text{ erg s}^{-1}$). The depth and spatial coverage of completed and ongoing surveys seem to rule out this possibility. Furthermore, to discover enough lower-luminosity bright sources ($L_x > 10^{35} \text{ erg s}^{-1}$) to bring the fraction of $L_x[0.3-7 \text{ keV}] > 10^{37} \text{ ergs s}^{-1}$ sources into line with the Galactic value (1/12), we would have to find ~ 200 such sources. In this case, the fraction of M31 GCs with X-ray sources would lie somewhere between 1/2–1. The contrast between this value and the value of $\sim 1/10$ for Galactic GCs which house bright X-ray sources, would itself prove interesting.

4.3. Spectral Comparisons

Since our data and analysis show that there are clear differences in the luminosity functions of the Galactic and M31 globular cluster X-ray sources, it is important to compare the source spectra as well. Because of the greater distance of M31, we can at present only compare the spectra of its most luminous clusters with the spectra of Galactic GC sources. In addition, the M31 GC X-ray spectra collected so far, even for these bright sources, generally have fewer counts, making direct comparison with the best Galactic GC data difficult. Furthermore, if some of the bright M31 GC sources we observe are actually composites of separate sources, blending may further complicate the comparisons. Despite these caveats, it is important to make a first step toward the systematic comparison of spectra. Future observations which can provide better spectral and spatial resolution will allow more detailed and meaningful comparisons to the model.

4.3.1. M31

We used the fits to the ACIS-S observations described in §3. All sources, except Bo 82, as seen in an ACIS-S observation on 2001 March 8, can be fitted by a single power law model with $\alpha = 1.4 - 1.9$. The Bo 82 spectra exhibited a somewhat harder ($\alpha = 1.1$) spectrum.

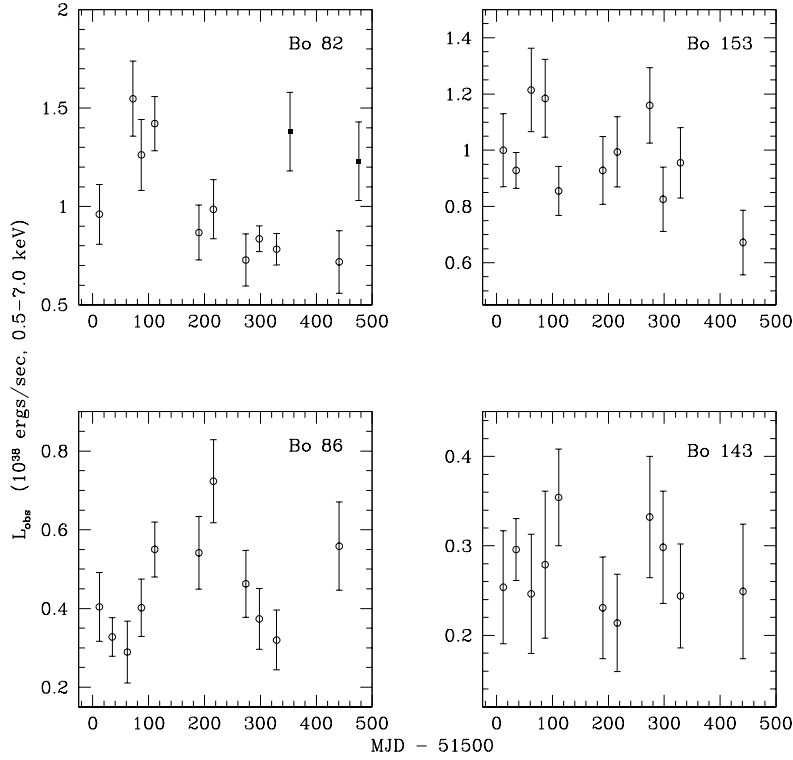


FIG. 7.— *Chandra* HRC light curves of Bo 82, Bo 153, Bo 86 and Bo 143. The two ACIS-S pointings of Bo 82 are also included in the plot (solid squares). The luminosity was estimated by the best-fitting spectrum which derived from ACIS pointings. To compute its luminosity, we assumed Bo 82 to be in its soft state ($\alpha = 1.4$).

Previous *BeppoSAX* observations provide another important resources. Trinchieri et al. (1999) showed that 8 of the M31 GC candidates spectra can be fitted with either a power law ($\alpha = 0.8 - 1.9$) or a bremsstrahlung ($kT = 6 - 9$ keV) model in 1.8–10 keV. Two of them (Bo 82 and Bo 158) have somewhat harder spectrum with $\alpha \sim 1$. Both the spectral fit of our Bo 82 data (§3) and the binned count rates shown in Table 4, demonstrate that these two sources are relatively harder than the others. Therefore the *BeppoSAX* observations appear to be consistent with ours, although source confusion could complicate the comparison.

4.3.2. Comparisons with the Milky Way

Callanan et al. (1995) found from archival *EXOSAT* data that 5 out of the 6 Galactic GCs can be well fitted with a power law plus blackbody spectral model ($\alpha = 1.6 - 2$, $kT = 0.5 - 1.5$ keV). Our high signal-to-noise Bo 375 spectra are consistent with their results.

In a recent study of GCs in our Galaxy using *BeppoSAX*, Sidoli et al. (2001) showed that the X-ray spectra of GCs can extend up to 20–100 keV and they can be fitted with a black-body (or disk black-body) plus Comptonization model. We here found the M31 GC sources also have hard X-ray tails up to ~ 10 keV (which is the limit of both *ASCA* and *Chandra*). We have also tried to fit the spectra of Bo 375 with COMPTT and COMPST models used by Christian & Swank (1997) and Sidoli et al. (2001); the parameters were not constrained and the Comptonizing plasma temperature (kT_e) has a very large value (~ 100 keV). This indicates that kT_e is above 10 keV, which is also seen in GCs in our Galaxy (e.g., Sidoli et al. 2001).

To facilitate the comparison between M31 sources and Galactic sources, we reanalyzed all the archival *BeppoSAX* Galactic GCs used by Sidoli et al. (2001). The reason for using *BeppoSAX* data is that it

covers more samples and has a common energy range with *Chandra*. We used an absorbed power law model (with N_H fixing at the optical determined value). We also restricted the fit to energies ranging from 2–7 keV for both data sets. The reason for this is that absorption plays a significant role in shaping the observed spectrum from some of the Galactic sources; we wished to compare the Galactic and M31 sources across a range of energies in which absorption is not important. Table 5 shows the results of the *BeppoSAX* spectral fits together with the *Chandra* fits on M31 sources in the same energy range. Although the fits are unacceptable for some cases, and are not expected to correspond to the true physical models, due to our limited energy range, the derived α is in the range of 1.4–2.5, while M31 sources have values between 1.4 and 1.9. These results are in good agreement, although the sample size of M31 sources is limited. We also used PIMMS to estimate the *Chandra* count rate for a single power law spectrum with $\alpha = 1.4 - 2$ and $N_H = 10^{21} \text{ cm}^{-2}$ and calculated the hardness ratio (2–10 keV/0.5–1.5 keV). The hardness ratio ranges from 0.4 to 0.8 which is consistent with most of the values shown in Table 4. Combining the M31 GC sources observed with *BeppoSAX* in 1.8–10 keV (Trinchieri et al. 1999), we conclude that the X-ray spectral properties of M31 GCs and Galactic GCs above 2 keV are roughly the same.

These comparisons make it clear that, in spite of significant luminosity differences, the conjecture that the M31 globular cluster X-ray sources have spectra similar to those of the Galactic GC sources is still viable. Nevertheless these broad band comparisons are not able to either establish a neutron star nature or rule out a black hole nature for the sources. The need for further observations is emphasized by the fact that observations of Bo 82 have found it to be sometimes in a luminous soft state, similar to Galactic GC sources, and sometimes in a luminous hard state.

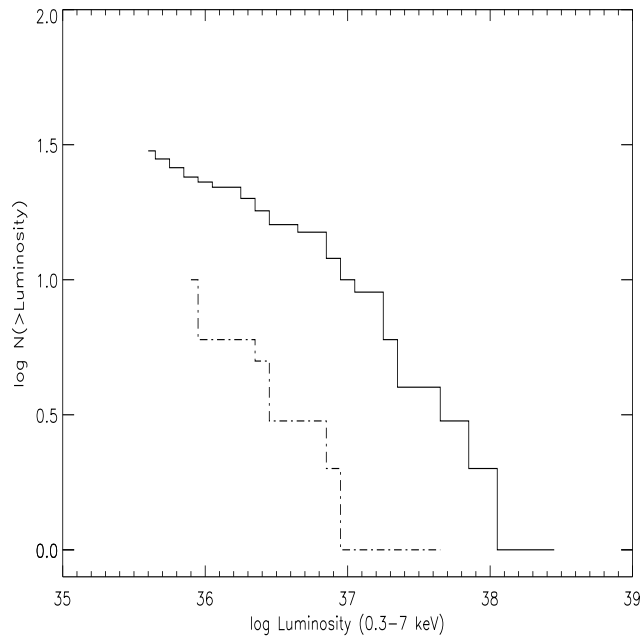


FIG. 8.— Luminosity functions for M31 globular clusters and Galactic clusters. The solid curve represents the M31 clusters and the dashed curve is the distribution of the Galactic sources (Verbunt et al. 1995).

TABLE 5
BEST-FIT SPECTRUM (2–7 keV) OF GALACTIC AND M31 GLOBULAR CLUSTERS

Source	Distance (kpc)	N_H (10^{21} cm^{-2})	α	χ^2_ν/dof
NGC1851	12.2	0.18	1.98 ± 0.05	1.3/51
Terzan 2	10.0	7.16	1.44 ± 0.04	15.9/51
NGC6441	10.7	2.32	1.63 ± 0.05	5.4/51
Terzan 6	7.0	13.24	1.82 ± 0.01	1.0/51
NGC6624	8.1	1.61	1.93 ± 0.03	3.2/51
NGC6712	6.8	2.51	2.46 ± 0.01	1.1/51
NGC7078	10.5	0.36	1.85 ± 0.09	8.3/50
NGC6440	7.0	6.27	1.62 ± 0.01	1.2/51
Terzan 1	5.2	12.17	2.00 ± 0.15	1.5/28
Bo 375	780	0.61	1.86 ± 0.05	0.96/115
Bo 82 (1st)	780	4.00	1.67 ± 0.09	0.81/57
Bo 82 (2nd)	780	4.00	1.32 ± 0.10	0.97/47
Bo 153	780	0.60	1.53 ± 0.19	1.02/14
Bo 86	780	0.44	1.43 ± 0.30	0.32/6
Bo 143	780	0.72	1.89 ± 0.75	0.37/1

NOTES — see §4.3.2 for discussion.

5. THE M31 GLOBULAR CLUSTER SYSTEM VS THE MILKY WAY'S CLUSTERS

The fact that X-ray binaries are as luminous as the ones we have studied in M31 globular clusters is not problematic. These sources do present a puzzle, however, when we compare them to globular cluster X-ray sources in our own Galaxy. The primary differences between the population of X-ray sources in M31 globular clusters and those in Galactic globular clusters are that (1) the peak luminosity is higher, and (2) the high-luminosity end of the distribution function is more populated. It is natural to ask if these differences can be explained by differences in the two galaxies' populations of globular clusters.

There is one obvious difference between the globular cluster systems of M31 and the Milky Way: M31 has more globular clusters. With ~ 150 well documented Galactic globular clusters, the total population could be larger by ~ 20 (Minniti 1995). The total number of M31 globular clusters is less certain, but there are over 200 confirmed clusters (Barmby et al. 2000) and the total population could be $\gtrsim 400$ (Battistini et al. 1993). On a practical level, the greater distance to clusters in M31 has made it difficult to learn as much about individual clusters as we know about Galactic globular clusters. HST has enabled studies of M31 globular cluster morphology (Bendinelli et al. 1993) and stellar populations (Ajhar et al. 1996), although not at the same level ground-based studies have achieved for globular clusters in our own Galaxy. HST studies, which have concentrated on the brightest M31 globular clusters, find no obvious differences between the properties of these clusters and those of the brightest Milky Way clusters. Ground-based observations of M31 globular clusters have provided a wealth of information about integrated luminosities, colors, and spectroscopic features of the population as a whole. The result of these studies is that the globular clusters of M31 are similar in most respects to those of the Galaxy. Differences tend to be subtle: for example, M31 GCs are overabundant in CN compared to Milky Way GCs of the same metallicity (e.g., Burstein et al. 1984). The M31 globular cluster luminosity function also shows evidence for variation not seen in the Milky Way GC luminosity function: the inner clusters are on average, brighter than the outer clusters, and the metal-rich clusters are brighter than the metal-poor clusters (Barmby, Huchra, & Brodie 2001). Assuming the GC luminosity function differences are real and not caused by catalog incompleteness, they could point to age or mass variations in the M31 GCs (see §6).

5.1. Fraction of Clusters with X-ray sources: Radial Dependence

Since we have imaged four fields at different locations in M31, we can examine the fraction of clusters with X-ray sources as a function of projected distance from the center of the galaxy. To do this, we used the GC catalogs to determine which clusters fell into the region of sky covered by each image. The number of X-ray detected clusters divided by the total number of clusters in each image is the fraction of clusters with X-ray sources.

Determining this fraction is not as straightforward as it seems: while the number of X-ray detected objects is well-understood, the number and identity of all true globular clusters in M31 is not. The true number of clusters in the central regions is particularly uncertain: globular clusters are difficult to detect against the bright, variable stellar background, and the existing catalogs may be incomplete. We therefore computed two fractions: the fraction of confirmed globular clusters detected as X-ray sources, and the fraction of all GC candidates detected. Since only a fraction of candidates are confirmed, and not all cluster candidates are true clusters, these two values should bracket the true fraction of M31 clusters with X-ray sources.

Figure 9 shows these fractions for each field as a function of the projected distance, R_p , from the center of M31. The figure also shows the fraction of Milky Way clusters with X-ray sources in four bins of R_p , where R_p was computed for each cluster as if the Milky Way globular cluster system were viewed from the same inclination angle as the M31 GCS. Although in M31 we have only four fields and 30 detected clusters, there is a clear decline in the fraction of M31 clusters with X-

ray sources as R_p increases, and a suggestion of the same effect in the Milky Way. The Milky Way curve is bracketed by the two M31 curves (the dip at the second point is probably not significant given the small number of Galactic X-ray sources), suggesting that the pattern in the two galaxies is similar. The decline in the number of X-ray sources as R_p increases can be understood if dynamical evolution drives the creation of X-ray binaries, since dynamical evolution is expected to be accelerated for clusters with orbits that bring them closer to the center of a galaxy.

The overall fraction of clusters with X-ray sources is fairly similar in the two galaxies. The Milky Way has 12 X-ray source clusters and a total of 147 clusters, so $\sim 10\%$ of clusters have X-ray sources. In our M31 fields, the fraction of confirmed clusters with X-ray sources is 25%, and the fraction of all cluster candidates with X-ray sources is $\sim 7\%$. Again, to within our admittedly large uncertainties, the fraction of clusters with X-ray sources seems to be fairly similar in the two galaxies. It is therefore tempting to view the combined Galactic and M31 globular clusters systems as a single population of clusters. In this view, the clusters in M31 can help us to learn more about conditions in Galactic globular clusters, mainly by providing a larger population of clusters to study.

5.2. Properties of Clusters with X-ray Sources

Do M31 GCs with X-ray sources differ from those without? We compared optical colors and apparent magnitudes, color excesses, metallicities, radial velocities, and positions of the two populations using data drawn from the Barmby et al. (2000) catalog. We also compared estimates of the core radii, from Crampton et al. (1985), and estimates of the clusters' ellipticities, from Staneva et al. (1996) and D'Onofrio et al. (1994) (these estimates are from ground-based optical imaging and are not particularly precise; their major advantage is that they are available for most of the clusters). A KS test was used to determine whether the two populations were drawn from the same distribution. The only significant difference between the X-ray source and non-X-ray-source clusters is in luminosity. The clusters with X-ray sources are brighter than the non-X-ray clusters, at the 99% confidence level. The luminosity difference of the median values is 0.55 magnitudes, or a flux difference of a factor of 1.7.

For 20 clusters (6 with X-ray sources and 14 without), structural parameters were also available from HST images (Barmby 2001). We compared the properties of the two groups and found only one significant difference: the central surface brightness of the X-ray source clusters was much brighter (median $\mu_{0,V} = 14.7$) than that of the non-X-ray-source clusters (median $\mu_{0,V} = 16.3$). This result is only significant at the 92% confidence level, and is based on a small number of objects. However, it is consistent with the above result, as studies of larger populations of M31 and Milky Way clusters show that more luminous clusters tend to have higher central surface brightnesses (Djorgovski & Meylan 1994; Barmby 2001).

We also compared the properties of M31 clusters with X-ray sources to those of Milky Way clusters with X-ray sources. The only possibly significant difference was in the luminosity: the M31 X-ray clusters were brighter in V than the Milky Way X-ray clusters. This is not true of the GC populations in general — the overall globular cluster luminosity functions are not significantly different — so it could be a clue to the M31 GCs' higher X-ray luminosities. It would be interesting to know whether the higher optical luminosities of the M31 X-ray GCs translate into higher masses; unfortunately, mass determinations from velocity dispersions are available only for a few M31 GCs, and only one of the X-ray sources. There are no clear correlations between M31 GC X-ray source luminosity and any of the cluster properties mentioned above.

6. CONCLUSION: POSSIBLE EXPLANATIONS

6.1. Individual Bright M31 GC Sources

Some individual X-ray sources in M31 globular clusters are significantly more luminous than any individual X-ray source yet observed

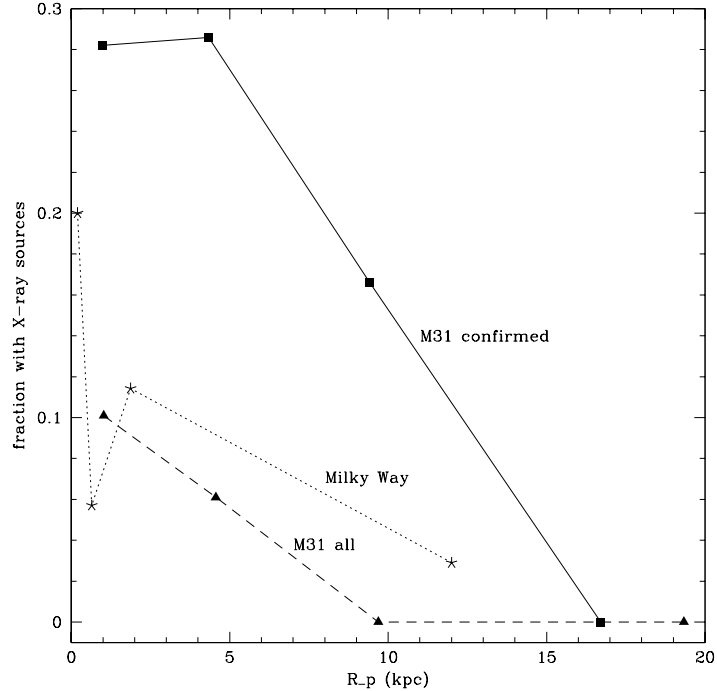


FIG. 9.— Fraction of GCs with bright X-ray sources as a function of projected separation, R_p , from the galaxy center.

in Galactic globular clusters. Bo 375 is an example. With changes in flux at the $\sim 50\%$ level over 16 hours and at the 100% level over times ranging from months to years, it seems clear that a single component must be contributing at least half of the X-ray energy emitted at typical times. This source would, by itself, approach the Eddington limit for a $1.4M_\odot$ neutron star, and must be more than twice as X-ray luminous as the maximum L_x measured for any Galactic globular cluster X-ray source. We find similar variability effects in the 500-day light curves of 2 other highly luminous M31 GC X-ray sources, Bo 82 and Bo 86. It may therefore be the case that the most luminous sources we observe in M31 GCs are either individual X-ray binaries (although there is evidence in the ACIS-S image that Bo 375 may not be a point source), or composites of a small number of independent X-ray binaries. An alternative explanation might apply to some of the sources not yet known to exhibit significant short-term variation: that some of the more luminous sources ($L_x > 5 \times 10^{37}$ ergs s^{-1}) are composed of a fairly large number (~ 10) of typical Galactic globular cluster X-ray binaries. Although not ruled out, such a large number of sources in roughly 1/4 of M31's globular clusters, with no composites at all yet observed in Galactic globular clusters, seems extreme (see §6.2).

It is clear that the physical characteristics of at least those very bright M31 GC sources exhibiting significant short-term variability differ from those of Galactic GC sources. We have therefore analyzed the spectra of the 5 brightest M31 sources (the only M31 GC sources for which we have collected more than 400 counts) and compared them, and also M31 GC X-ray sources studied previously with *BeppoSAX* (Trinchieri et al. 1999), with the spectra of Galactic sources. The spectra are similar to those of Galactic GC sources, but 2 sources exhibit somewhat harder power-law tails; one of these appears to make transitions between a soft and a hard state. It is not possible to draw conclusions about the physical nature of the sources from these crude comparisons (which are nevertheless, the best presently possible). We must therefore continue to carry out time variability and spectral studies that could possibly, in combination, tell us whether each source is an accreting black hole or neutron star. High-spatial resolution ob-

servations with these sources on-axis, and spectra from longer observations with *Chandra* and *BeppoSAX* could play important roles, as could *XMM-Newton* and HST observations. Progress along theoretical lines could also help to distinguish signatures of a relatively steady black hole accreter from those of a neutron star accreter.

If it is an accreting black hole, the time signatures of the source in Bo 375 are more characteristic of a persistent, rather than a transient source. Although this would at first suggest a high-mass ($M > 5M_\odot$) donor, such a donor is unlikely to be found in a globular cluster—even if the cluster is relatively young and even if the rate of stellar interactions near the cluster core is high. Nevertheless, if a low-mass donor is evolving away from the main sequence, a black hole accreter that might otherwise be transient could be highly luminous over relatively long times.

Below we construct a specific neutron star model for Bo 375 suggested by the 16 hour time scale observed by *ROSAT*. This model may or may not describe the actual physics of Bo 375, but it is consistent with the data and could apply to other bright GC sources in the youngest clusters of M31 and other galaxies.

6.1.1. A Model for Bo 375

The spectral and timing studies we have been able to carry out so far have not provided promising clues as to the nature of this X-ray source (or sources). It is intriguing, however, that *ROSAT* observations found what appeared to be systematic, possibly periodic, variations on a time scale of ~ 16 hours. If these variations are associated with an orbital period, this would suggest that mass transfer is occurring on the thermal-time-scale of a slightly evolved Roche-lobe filling star.

6.1.2. Thermal Time Scale Mass Transfer

Thermal-time-scale mass transfer is driven by the reaction of a Roche-lobe-filling donor star to mass loss (van den Heuvel et al. 1992; Kalogera & Webbink 1996; Di Stefano & Nelson 1996; King et al. 2001; King & Begelman 1999). Consider a donor star which would, were it living in isolation, have an equilibrium radius R_{eq} determined

by its total mass and state of evolution. If this star is in a close binary and is filling its Roche lobe, in a situation in which R_L is consistently somewhat smaller than R_{eq} , then the drive of the star to achieve equilibrium causes it to lose mass through the L1 point at a relatively rapid rate. In fact, if the ratio of the donor mass to the accretor mass is too large, or if the donor is evolved enough to be fully convective, the mass transfer process can become dynamically unstable, leading to the formation of a common envelope. If, however, a dynamical instability is avoided, mass transfer is driven on a time scale closely related to the thermal time scale of the donor.

In general, the two assumptions of a Roche-lobe filling donor and angular momentum conservation lead to an analytic expression for \dot{m} , the rate at which the donor loses mass. This expression can be written generically as

$$\dot{m} = \frac{\mathcal{N}}{\mathcal{D}}, \quad (1)$$

where \mathcal{N} and \mathcal{D} are each generally functions of the masses of the donor and accretor; the state of evolution of the donor, which can be parameterized by its core mass, m_c ; β , the fraction of the mass incident on the accretor that is actually retained; parameters that quantify the amount of angular momentum dissipated or else carried away by matter ejected from the system; and the orbital separation a between the components of the binary. The value of \mathcal{D} determines whether mass transfer can be dynamically stable.

The numerator is a sum of terms: \mathcal{N}_w is related to the donor's stellar winds; \mathcal{N}_{gr} and \mathcal{N}_{mb} are governed by gravitational radiation and magnetic braking, respectively; \mathcal{N}_{nuc} relates to the nuclear evolution of the donor; \mathcal{N}_{th} relates to the thermal-time-scale readjustment of the donor to the size of the Roche lobe. Different regions in the parameter space correspond to different physical systems. For example, mass transfer in systems with large values of m_c and a is driven by the nuclear evolution of the system; \mathcal{N}_{nuc} is the dominant term.

\mathcal{N}_{th} can be the dominant term when the donor's mass is comparable to or greater than that of the accretor, especially when the donor is somewhat evolved, but does not yet have a fully convective envelope (typically $0.05M_\odot < m_c < 0.2M_\odot$). Orbital periods are typically on the order of a day. In such cases, the rate of mass transfer can be expressed as

$$\dot{m} \sim \left(\frac{R_{eq} - R_L}{R_{eq}} \right) \left(\frac{1}{\tau_{KH}} \right) \mathcal{F}_{dyn} \mathcal{G}_{star} \quad (2)$$

In the expression above, τ_{KH} is the Kelvin-Helmholz time of the donor star ($\sim 10^7$ years for a star of approximately M_\odot); \mathcal{F}_{dyn} is a factor that depends on the mass ratio of the stars and on the amount of angular momentum carried away by any mass exiting the system or else lost through dissipative processes like gravitational radiation; \mathcal{G}_{star} expresses the donor's response to mass loss; this factor must be computed by a Henyey-like calculation. The favored values for the calculations we present below are taken from work by Nelson (1995). For more details about this type of mass transfer (see Di Stefano & Nelson (1996) and references therein).

6.1.3. System Properties

When the accretor is a neutron star, only a narrow range of donor masses and states of evolution (as specified by the helium core mass) will permit dynamically stable mass transfer driven on the thermal time scale of the donor. In Figure 10 we have shown the range of system parameters for such systems at that point in their evolution at which P_{orb} is 16 hours and the accretion rate onto a neutron star companion has just increased to $10^{-8}M_\odot$. Donor masses range from $1.1 - 1.6M_\odot$ and donor core masses are near $0.11M_\odot$.

6.1.4. Evolution

Although we don't know that the 16-hour time variability of Bo 375 is related to an orbital time scale, it is reasonable to entertain this possibility. To this end we computed the evolution of tens of thousands of

systems. Shown in Figure 11 are the results of some typical evolutions of binaries that would have accretion energies greater than 10^{38} ergs s^{-1} during a time interval in which their orbital periods are 16 hours. Note that during the early parts of the evolution, the donor's radius (which is governed by its total mass is also influenced by its core mass), and the orbital period can decrease.

6.1.5. Viability in a Globular Cluster Environment

This sort of scenario has not been considered for neutron stars in GCs, because the required mass of the donor star is larger than the mass of stars at the turn-off of typical Galactic GCs (Di Stefano & Davies 1996 have considered such a scenario for white dwarfs; see Hertz, Grindlay, & Bailyn 1993; Verbunt et al. 1994, 1995). There are two sets of circumstances, however, that alone or in combination can provide a pool of massive donor stars. The first and simplest is a younger cluster age. Although most Galactic GCs seem to have been formed between 12 and 15 Gyr ago, other galaxies may have experienced several distinct epochs of globular cluster formation. This seems to have been the case in the Magellanic Clouds (see, e.g., Da Costa, Mould, & Crawford, 1985), and is also expected in galaxies that have experienced interactions with neighboring galaxies. We do not know if M31 contains GCs formed during different epochs, but Barmby, Huchra, & Brodie (2001) have suggested that the difference in optical luminosity between the inner and outer GCs in M31 can be explained if the brighter clusters are $\sim 55\%$ younger than the fainter clusters. Young clusters formed 7 – 9 Gyr ago could harbor slightly evolved stars that would fit the criteria shown in Figure 10 for a thermal-time-scale mass transfer system with a 16 hour period.

In addition, a relatively high probability of interactions enhances the probability of finding a massive star in a close orbit with a neutron star. If, for example, interactions among massive stars in the core region have led to stellar mergers, thermal-time-scale mass transfer onto a neutron star could be expected to occur in GCs.

6.1.6. Tests

One test of the applicability of our model to individual bright sources in M31 would be the discovery of time ~ 1 day variations among the M31 GC sources (or in other galaxy's GCs) that can be reasonably linked to an orbital period. Another test can be applied to galaxies with GC systems that house highly luminous sources that are candidates for our model: are the relative numbers of systems of different luminosities consistent with the lifetimes of the corresponding phases of binary evolution? We find, for example, that the epoch during which the luminosity remains above 10^{38} ergs s^{-1} is approximately 10^7 years, roughly τ_{KH} for the donor. The lifetime of the accretion luminosities above 10^{37} ergs s^{-1} are ~ 10 times longer. This roughly matches the statistics of the M31 GC sources. Finally, as we probe the globular cluster systems of more distant galaxies, we can search for correlations between the X-ray luminosities of GCs and the ages of GCs. While no individual test is likely to be definitive, a combination of them could provide support for, or else falsify, the model.

6.2. Other M31 Globular Clusters

This paper started as a description of an interesting X-ray luminous globular cluster, Bo 375, which happened to be in the field of view of a *Chandra* census of M31. Its high luminosity, together with indications that the source is not point-like, attracted our attention to this cluster. The fact that others of the most luminous sources studied in the census are also associated with globular clusters led us to extend our investigation and to find that the high-end of the the GC X-ray source luminosity function has a higher peak luminosity and a larger fraction of all sources populating the region with $L_x > 10^{37}$ ergs s^{-1} . The fundamental issue we address in this section, is why M31's globular clusters should be more likely than those of our own Galaxy to house brighter X-ray sources and multiple X-ray sources. We find that three effects are likely to be at work.

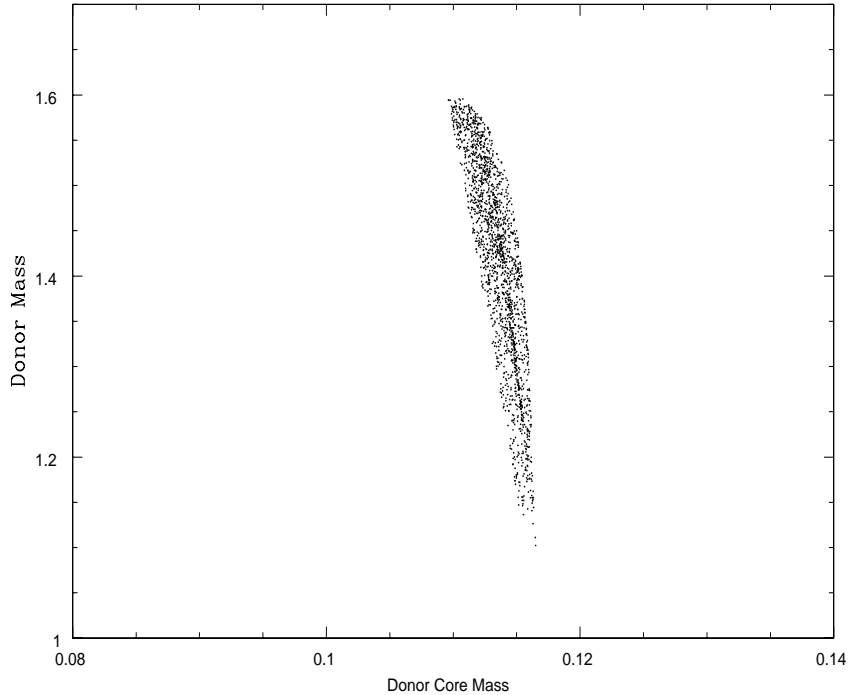


FIG. 10.— Each dot corresponds to a physical system with an orbital period of 16 hours, and an accretion luminosity above 10^{38} erg s $^{-1}$.

6.2.1. Possible Explanations: I. Large Population of Clusters

Let us entertain the hypothesis that the Milky Way and Andromeda globular clusters are members of a single distribution of clusters. In this case, the total population of clusters could be ~ 550 . We certainly wouldn't expect that every possible cluster phenomenon could be discovered in the arbitrary subset of 150 that we happen to find in our own Galaxy. If, e.g., black hole binaries are only 1/20 as likely to form and remain in clusters as are neutron star binaries, we would have a small chance of observing one among the 14 MW GCs with X-ray sources, but would have an improved chance of discovering one in the ~ 50 X-ray active GCs in M31. Unfortunately, however, we have no *a priori* estimates of the probability of events (such as the formation of a black-hole binary) that (a) have never been observed, and that (b) are not readily amenable to reliable first-principles predictions. Thus, all that can be said is that we should perhaps not be too surprised if some of M31's GCs do contain actively accreting black holes, or unusually massive (e.g., $2-3 M_{\odot}$) accreting neutron stars, or even unusually massive donor stars.

There is, however, one yet-to-be-observed GC situation, for which the probability can be estimated. This is the situation in which a cluster houses more than one bright X-ray binary. If p represents the probability of finding an X-ray source in a GC, Poisson statistics predict that, for every GC with a single X-ray source, there should be $p/2$ clusters with 2 sources and $p^2/6$ clusters with 3 sources. If $p \sim 0.1-0.2$, we would predict that 3–5 GC X-ray sources in M31 should be composites of 2 independent sources, while fewer than 1 is likely to be composed of 3 independent sources.

One can also attack this question of the probability of multiplicity from the perspective of the probability of the 2-, 3-, and 4-body processes that produce X-ray binaries. What is the probability that two interactions will produce 2 independent X-ray sources that are active at the same time? Such a question certainly can be well posed and answered subject to input assumptions about the lifetimes of X-ray binaries. Since, however, current estimates of the lifetime of X-ray activ-

ity vary by 1–2 orders of magnitude, the most reliable answer comes from the phenomenology that allows us to estimate p . It is important to note, however, that if a subset of clusters have different physical characteristics, the true probability of observing multiple X-ray sources in these GCs could be different,

6.2.2. Possible Explanations: II. More Highly Evolved Clusters

Although there are striking similarities between the MW and Andromeda galaxies, they are not identical. In fact there are differences that are likely to lead to more or (“enhanced”) accelerated evolution of GCs close to the center of M31 than of clusters close to the center of the MW. According to van den Bergh (2000), the nuclear mass of M31 is almost 30 times larger than the nuclear mass of the MW ($7 \times 10^7 M_{\odot}$ vs $2.5 \times 10^6 M_{\odot}$). The bulge dispersions are 155 km/s and 130 km/s, respectively, while the rotational velocities are, respectively, 260 km/s vs 220 km/s. All of these differences indicate that GCs close to the center of M31 are likely to evolve more quickly than clusters close to the center of our Galaxy (see, e.g., Gnedin, Lee, & Ostriker 1999, and references therein). Since cluster evolution leads to smaller and denser cores, at least until the onset of core collapse, the conditions that lead to the formation of X-ray binaries may also be enhanced, leading to more X-ray binaries in M31 GCs. Certainly the fact that there are more X-ray luminous clusters closer to the centers of both M31 and the MW speaks in favor of the role of accelerated evolution. The apparent dearth of low-mass clusters near the center of M31 (Barmby, Huchra, & Brodie 2001) has also been taken as evidence in favor of the role of accelerated evolution. There is one discrepancy, however, in that the observed velocity dispersions in M31 are not consistent with theoretical calculations of accelerated evolution (Barmby, Huchra, & Brodie 2001).

There is an argument that may not favor enhanced accelerated evolution as the primary reason for the brighter X-ray luminosities of M31 GCs. This is that, so far, the fraction of M31 globular clusters in each region of the galaxy seem comparable to the fraction observed at sim-

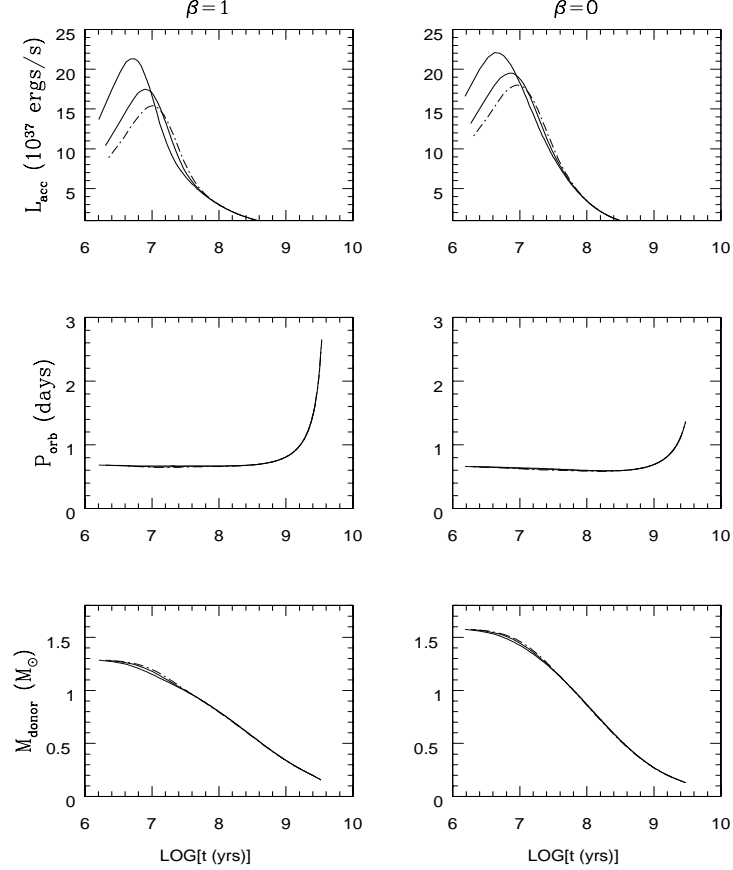


FIG. 11.— Evolution of a typical system which has accretion luminosity above 10^{38} erg s $^{-1}$ during a time when its orbital period is 16 hours. $\beta = 1$: In this case, the neutron star accretes all of the incident matter. If, however, $\beta = 1$ would produce super-Eddington accretion, the value of β is calculated in an internally-consistent way (see Di Stefano 2001). Note that for non-zero β , the mass of the neutron star can increase. $\beta = 0$: the mass of the neutron star is held constant. In both cases the middle curve was computed using the values for the thermal time-scale readjustment of the donor computed by Nelson (1995). The upper and lower curves tested the effects of altering these values (which are uncertain) by about an order of magnitude.

ilar values of R_p for the MW. As we have pointed out, these results are subject to significant uncertainties. But, if it is true that the fraction of GCs with X-ray sources is indeed comparable for comparable values of R_p , this would appear to limit the role of enhanced accelerated evolution. It could, however, still be invoked to explain higher cluster X-ray luminosities in M31 through the formation of more or brighter binaries if, e.g., the time scale for X-ray emission is only a short fraction of the cluster's orbital period.

In summary, it is difficult to quantify the role of accelerated evolution due to interaction of M31's GCs with the rest of the galaxy. Nevertheless, it is likely that it does play a somewhat different role in M31 than in the MW, simply because of the differences in mass and mass distribution in the 2 galaxies. If, therefore, we wish to view the two systems of globular clusters as a single larger system of some 400–550 clusters, we must invoke the proviso that none of the Galactic clusters experience tidal and disk interactions as extreme as those experienced by clusters which pass close to the center of M31. That is, if we were to map Galactic clusters onto M31, in such a way that their interactions with M31 would mimic the conditions each actually experiences due to the Milky Way, the Galactic clusters would generally be placed farther from the center of M31 than their actual distance from the center of the Galaxy. Thus, M31 may be expected to contain not only globular clusters with properties that are similar to those found in our Galaxy, but also a sub-population whose evolution is proceeding at a more rapid pace due to interactions with M31; these more rapidly evolving clusters are most likely to be found near the center of M31.

Note that if enhanced accelerated evolution is responsible for the more luminous GC X-ray sources in M31, then M31 GCs with bright X-ray sources should have different structure parameters. HST observations could therefore help to determine the role of enhanced accelerated evolution.

6.2.3. Possible Explanations: III. Younger Clusters

Barmby, Huchra, & Brodie (2001) have suggested that the difference in optical luminosity between the inner and outer GCs in M31 (i.e., the clusters with smaller projected distance from the center vs those with larger values of R_p) can be explained if the brighter clusters are $\sim 55\%$ younger than the fainter clusters. This may be relevant to the M31 GCs with X-ray sources, because we have found that these clusters tend to be optically brighter than clusters without X-ray sources. If the turn-off in most GCs is at $\sim 0.8M_\odot$, the turn-off in the more massive clusters would be at about $\sim 1.1 - 1.2M_\odot$. It is much more likely to find a donor with high-enough mass for thermal-time-scale mass transfer to occur in a GC with a turn-off at $\sim 1.1M_\odot$. This can be easily understood by noting that all of the low-probability interactions that could produce such a binary in an old cluster, are supplemented by a wealth of additional interactions involving stars of relatively high mass. Furthermore, there is a clear prediction that thermal mass transfer is much more likely in younger clusters. Calculations are underway to quantify this effect.

6.3. Conclusions

M31 globular clusters could have turned out to have X-ray properties almost exactly like those of the Milky Way. In this case, studies of M31 would have told us more about the processes that go on in our own Galaxy, simply because their larger numbers provide a bigger arena for the relevant interactions to occur. M31 globular clusters could have turned out to have X-ray properties very different from those of the Milky Way. In this case they might have provided a gateway to our understanding of GCs in external galaxies.

The population of M31 GCs did turn out to be include clusters that appear to have similar X-ray properties to those of the MW, as well as a significant subset that have different X-ray properties. Perhaps this is the best of both worlds, because we can now hope to learn about processes occurring in our own GCs, and also about processes that do not occur here or occur only with very low probability.

For example, we might expect to find highly-luminous thermal-time-scale mass transfer systems in galaxies with populations of young clusters, and none such in galaxies such as our own, with only old

populations of stars in GCs. Thus, the relevance of the thermal-time-scale model we have introduced, can be tested by determining whether galaxies thought to include more recently formed GCs have more highly luminous GC X-ray sources. Similarly, the importance of interactions with the host galaxy can be tested by comparing GC X-ray sources in galaxies that have more massive bulges with GC X-ray sources in galaxies with less massive bulges.

In short, *Chandra*'s investigation of the M31 GC system has provided puzzles that suggest many lines of investigation for the further study of M31's GCs, GCs in external galaxies, and theoretical work on binary formation and evolution in globular clusters.

We gratefully acknowledge thoughtful input from Anil Dosaj, Lars Hernquist, Margarita Karovska, Vicky Kalogera, Christopher Kochanek, Jeffrey McClintock, and Andrea Prestwich. This work was supported in part by NASA under GO1-2091X; A.K.H.K. is supported by a Croucher Fellowship.

REFERENCES

Ajhar, E., et al. 1996, AJ, 111, 1110
 Barmby, P., 2001, PhD thesis, Harvard University
 Barmby, P., Huchra, J.P. & Brodie, J.P. 2001, AJ, 121, 1482
 Barmby, P., Huchra, J.P., Brodie, J.P., Forbes, D.A., Schroder, L.L. & Grillmair, C.J. 2000, AJ, 119, 727
 Barret, D., Olive, J.F., Boirin, L., Done, C., Skinner, G.K., & Grindlay, J.E., 2000, ApJ, 533, 329
 Battistini, P., et al., 1987, A&AS, 67, 447
 Battistini, P.L., Bönoli, F., Casavecchi, M., Ciotti, L., Federici, L. & Fusi Pecci, F. 1993, A&A 272, 77
 Bendinelli, O. et al., 1993, ApJ, 409, L17
 Blöser, P.F., Grindlay, J.E., Kaaret, P., Zhang, W., Smale, A.P., & Barret, D., 2000, ApJ, 542, 1000
 Burstein, D., Faber, S.M., Gaskell, C.M. & Krumm, N. 1984, ApJ 287, 586
 Callanan, P., Penny, A.J., & Charles, P.A., 1995, MNRAS, 273, 201
 Charles, P., 1998, in proceeding of 'Observational Evidence for the Black Holes in the Universe', p. 279
 Christian, D.J. & Swank, J.H., 1997, ApJS, 109, 177
 Christian, D.J., Smale, A.P., Swank, J. H., & Serlemitsos, P.J., 1997, ApJ, 477, 424
 Church, M.J., & Balucinska-Church, M., 2001, A&A, 369, 915
 Clark, G.W., 1975, ApJ, 199, L143
 Crampton, D., Cowley, A.P., Schade, D. & Chayer, P. 1985, ApJ, 288, 494
 Da Costa, G. S., Mould, J. R., & Crawford, M. D. 1985, ApJ, 297, 582
 Deutsch, E.W., Margon, B., & Anderson, S.F. 2000, ApJ, 530, L21
 Di Stefano, R., & Rappaport, S., 1994, ApJ, 423, 274
 Di Stefano, R., & Nelson, L.A., 1996, in *Supersoft X-ray Sources*, refereed proceedings of the 1st Workshop on Supersoft Sources, ed. J. Greiner, Springer-Verlag, Berlin
 Di Stefano, R., & Davies, M.B. 1996, in *Supersoft X-ray Sources*, Proceedings of the 1st Workshop on Supersoft Sources, ed. J. Greiner, Springer-Verlag, Berlin
 Di Stefano, R., 2001, in preparation
 Dickey, J.M., & Lockman, F.J., 1990, ARA&A, 28, 215
 Djorgovski, S. & Meylan, G. 1994, AJ, 108, 1292
 D'Onofrio, M., Capaccioli, M., Wagner, S.J. & Hopp, U. 1995, Memorie della Societa Astronomica Italiana, 65, 731
 Dubath, P. & Grillmair, C.J. 1997, A&A, 321, 379
 Fabbiano, G., 1988, ApJ, 325, 544
 Garcia, M.R., Murray, S.S., Primini, F.A., Forman, W.R., Jones, C. & McClintock, J.E., 2000, proceeding of IAU Symp 205, 'Galaxies at the Highest Angular Resolution', in press (astro-ph/0012387)
 Gnedin, Y., Lee, H. M., & Ostriker, J. P. 1999, ApJ, 522, 935
 Grindlay, J.E., Heinke, C., Edmonds, P.D., & Murray, S.S., 2001, Science, in press (astro-ph/0105528)
 Guainazzi, M., Parmar, A.N., Segreto, A., Stella, L., Dal Fiume, D., Oosterbroek, T., 1998, A&A, 339, 802
 Hakala, P.J., et al., 1997, MNRAS, 285, 693
 Hertz, P., & Grindlay, J., 1983, ApJ, 275, 105
 Hertz P., Grindlay J., Bailyn C., 1993, ApJ, 410, L87
 Huchra, J.P., Brodie, J.P., & Kent, S.M., 1991, ApJ, 370, 495
 Irwin, J.A., & Bregman, J.N., 1999, ApJ, 510, L21
 Kalogera, V., Webbink, R.F. 1996, ApJ, 458, 301
 King, A.R., Davies, M.B., Ward, M.J., Fabbiano, G., & Elvis, M. 2001, ApJ, 552, L109
 King, A.R., & Begelman, M.C. 1999, ApJ, 519, L169
 Kulkarni, S. R., Hut, P., McMillan, S. 1993, Nature, 364, 421
 Magnier, E. A., 1993, PhD Thesis, Massachusetts Institute of Technology
 Minniti, D. 1995, AJ, 109, 1663
 Nelson, L.A. 1995, private communication
 Primini, F.A., Forman, W., & Jones, C. 1993, ApJ, 410, 615
 Primini, F., Garcia, M., Murray, S., Forman, W., Jones, C., & McClintock, J., 2000, proceeding of 'The Interstellar Medium in M31 and M33', in press (astro-ph/0012164)
 Sargent, W.L.W., Kowal, C.T., Hartwick, F.D.A., & van den Bergh, S., 1977, AJ, 82, 947
 Sidoli, L., Parmar, A.N., Oosterbroek, T., Stella, L., Verbunt, F., Masetti, N., Dal Fiume, D., 2001, A&A, 368, 451
 Sigurdsson, S., Hernquist, L. 1993, Nature, 364, 423
 Supper, R., et al., 1997, A&A, 317, 328
 Supper, R., et al., 2001, A&A, in press (astro-ph/0104297)
 Staneva, A., Spassova, N. & Golev, V. 1996, A&AS, 116, 447
 Tanaka, Y., Shibasaki, N. 1996, ARA&A, 34, 607
 Tanaka, Y., Inoue, H., & Holt, S.S., 1994, PASJ, 46, L37
 Trinchieri, G., Israel, G.L., Chiappetti, L., Belloni, T., Stella, L., Primini, F., Fabbiano, P., & Pietsch, W., 1999, A&A, 348, 43
 van den Bergh, S. 2000, *The Galaxies of the Local Group*, Cambridge University Press
 van den Heuvel, E.P.J., Bhattacharya, D., Nomoto, K., Rappaport, S.A., 1992, A&A, 262, 97
 van Paradijs, J. 1996 ApJ 464L, 139.
 Verbunt, F., et al., 1995, A&A, 300, 732
 Verbunt F., Johnston H., Hasinger G., Belloni T., Bunk W., 1994, MmSAI 65, 249
 Verbunt F., Bunk W., Hasinger G., Johnston H., 1995, A&A 300, 732
 White, N.E., Stella, L., Parmar, A.N., 1988, ApJ, 324, 363